NASA TECHNICAL MEMORANDUM

NASA TM X-2516

NASA TM X-2516

EXPLORATORY INVESTIGATION OF FACTORS AFFECTING THE WING TIP VORTEX

by James Scheiman, James L. Megrail, and James P. Shivers

Langley Research Center

Hampton, Va. 23365

NATIONAL AERONAUTICS AND SPACE ADMINISTRATION • WASHINGTON, D. C. • APRIL 1972

1. Report No. NASA TM X-2516	2. Government Accession No.	3. Recipient's Catalog No.
4. Title and Subtitle EXPLORATORY INVESTIGATION OF FACTORS AFFECTING THE WING TIP VORTEX		5. Report Date April 1972 6. Performing Organization Code
7. Author(s) James Scheiman; James L. Megrail, Langley Directorate, U.S. Army Air Mobility R&D Laboratory; and James P. Shivers		8. Performing Organization Report No. L-8104 10. Work Unit No. 760-76-01-04
9. Performing Organization Name and Address NASA Langley Research Center Hampton, Va. 23365		11. Contract or Grant No. 13. Type of Report and Period Covered Technical Memorandum
12. Sponsoring Agency Name and Address National Aeronautics and Space Administration Washington, D.C. 20546		14. Sponsoring Agency Code

15. Supplementary Notes

Technical Film Supplement L-1113 available on request.

16. Abstract

An investigation was conducted in the Langley full-scale tunnel to study some factors affecting the tip vortex of a wing. It was found that there was a pronounced effect of Reynolds number on the tip-vortex core size. An attempt was made to determine what aerodynamic parameters – such as lift, drag, or induced drag – influence the size of the vortex core, but no particular function of the parameters was found to be superior to all others. Various spoilers placed on the upper and lower surfaces of the wing to increase the boundary-layer thickness resulted in a reduction in the vorticity as determined from the tuft grid. Various solid objects placed in the vortex core downstream of the wing tip seemed to decrease the vorticity within the vortex core.

17. Key Words (Suggested by Author(s))	18. Distribution Statement
Tip vortex Vortex core size Wind-tunnel tests Vortex structure Reynolds number effect	Unclassified – Unlimited

19. Security Classif. (of this report)	20. Security Classif. (of this page)	21. No. of Pages	22. Price*
Unclassified	Unclassified	50	$3.00

*For sale by the National Technical Information Service, Springfield, Virginia 22151

EXPLORATORY INVESTIGATION OF FACTORS AFFECTING THE WING TIP VORTEX

By James Scheiman, James L. Megrail,*
and James P. Shivers
Langley Research Center

SUMMARY

An investigation was conducted in the Langley full-scale tunnel, mainly by means of a tuft grid, to study some factors affecting the tip vortex of a wing. Measurements made at a distance of 5 chord lengths downstream from the wing showed that there was an effect of Reynolds number on the size of the tip-vortex core, the core being about the same size for Reynolds numbers between 1.2×10^6 and 1.9×10^6 but being markedly smaller for a Reynolds number of 0.8×10^6. An attempt was made to determine what aerodynamic parameters – such as lift, drag, or induced drag – influence the size of the vortex core, but no particular function of these parameters was found to be superior to the others. The implication is that the core size must be determined more accurately or it must be determined by parameters other than those investigated. Various spoilers placed on the upper or lower surfaces of the wing to increase the boundary-layer thickness resulted in a reduction in the core vorticity, as determined from the tuft grid, which result seems to be contrary to some hypotheses that the wing boundary layer forms the vortex core. Various solid objects placed in the vortex core downstream of the wing tip seemed to decrease the vorticity within the vortex core. The most promising such object seemed to be a small vane of about 1.5 percent of the area of the wing semispan, located with the surface of the vane alined with the free stream.

INTRODUCTION

A fundamental understanding of the structure of the helicopter rotor-blade tip vortex and a means of controlling it are of particular importance with regard to reduction of rotor-blade noise and dynamic loads. Unfortunately, there is no clear understanding of the structure of the tip vortex, and also the factors that affect it are not well known. The present investigation was conducted in an attempt to provide information to aid in the general study and possible alleviation of the trailing tip-vortex problem. Also, a review

---

*Langley Directorate, U.S. Army Air Mobility R&D Laboratory.

of the literature indicates that a large portion of the published work has been performed on small-scale models with very little attention given to scale or Reynolds number effects. Hence the present investigation, which was conducted at fairly large scale, also includes an attempt to determine whether there are any significant scale effects.

In attempting to modify the tip vortex, one of the desired engineering goals is to minimize the induced tangential velocities associated with the circulation of the vortex core. It has generally been supposed that the tangential velocities would be decreased if the size of the vortex core could be increased but, unfortunately, there is no common understanding of what parameters determine the vortex core size. Reference 1 states that the boundary layer shed from the trailing edge is turbulent, and it is this boundary layer that forms the vortex sheet that ultimately rolls up into the core. Using energy techniques (ref. 2) indicates that for an elliptical spanwise loading the core diameter is directly proportional to the wing span. Reference 3 indicates that the core diameter increases in direct proportion to the lift coefficient.

In an effort to obtain a clearer understanding of the structure of the tip vortex and to gain some insight into the Reynolds number effects, a semispan wing was tested in the Langley full-scale tunnel at Reynolds numbers from 0.8×10^6 to 1.9×10^6. Numerous full-span and semispan spoilers were tested in an attempt to affect the wing boundary-layer thickness and thus, hopefully, to affect the tip-vortex core size. It should be realized that the tip vortex of a fixed wing does not accurately represent the vortex of a rotor blade, but it was believed that fixed-wing tests would show up significant variations in the tip vortex.

The results of this investigation are presented mainly in the form of tuft-grid photographs. In addition to these photographs, motion-picture film supplement L-1113 has been prepared of smoke-flow tests. A request card and a description of the film are included at the back of this document.

SYMBOLS

Values are given in both SI and U.S. Customary Units. The measurements and calculations were made in the U.S. Customary Units.

A,B,C,E	constants
b	wing span, m (ft)
C_D	wing drag coefficient, D/qS

C_L wing lift coefficient, L/qS

c wing chord, m (ft)

D wing drag force, N (lb)

D_c tip-vortex core diameter, m (ft)

$\frac{D_c}{c}$ core-diameter—wing-chord ratio corresponding to each variable value (data point), referred to as core-diameter ratio

$\frac{D_c'}{c}$ core-diameter ratio determined from least-square-fit straight line corresponding to each variable value

$\overline{\left(\frac{D_c}{c}\right)}$ average core-diameter ratio determined by averaging the data

L wing lift force, N (lb)

q dynamic pressure, $\frac{1}{2}\rho V^2$, N/m^2 (lb/ft^2)

R effective Reynolds number, $1.1(Vc/\nu)$

r correlation coefficient

$$r^2 = 1 - \frac{\sum\left(\frac{D_c}{c} - \frac{D_c'}{c}\right)^2}{\sum\left[\frac{D_c}{c} - \overline{\left(\frac{D_c}{c}\right)}\right]^2}$$

S wing area, m^2 (ft^2)

V free-stream velocity, m/sec (ft/sec)

V_t tangential velocity around the tip-vortex core, m/sec (ft/sec)

α angle of attack, deg

Γ wing tip circulation, $\left(L\middle/\frac{\pi b}{4}\right)\middle/\rho V$, m^2/sec (ft^2/sec)

ν kinematic viscosity, m^2/sec (ft^2/sec)

ρ air density, kg/m^3 $(slugs/ft^3)$

APPARATUS AND TESTS

This test program was conducted in the Langley full-scale tunnel which has a test section 9 by 18 m (30 by 60 ft). The semispan wing was installed on the tunnel scale system with its span axis vertical. The wing angle of attack was varied by rotating the wing about its quarter-chord axis. An angle-of-attack drive servo and potentiometer were used to vary and measure the wing angle of attack. In order to provide clearance for the wing angle-of-attack drive system and to insure that the wing was above the ground-board boundary layer, the wing root end was mounted 15.88 cm $\left(6\frac{1}{4}\text{ in.}\right)$ above the wind-tunnel ground board. A small end plate (0.61 by 0.91 m (2 by 3 ft)) was installed on the wing root end to simulate a semispan wing. A photograph of the semispan wing in the wind tunnel is shown in figure 1. The model aerodynamic forces were measured on the tunnel scale balance system and recorded on a magnetic-tape system. The tip-vortex cross-sectional characteristics were obtained from photographs of a tuft grid. A sketch of the photographic system is shown in figure 2. A smoke generator was used at times to obtain a visual display of the tip-vortex fluid motion.

Model

The wing model had an NACA 0012 airfoil section with a span of 2.13 m (7 ft) and a chord of 0.61 m (2 ft). The wing tip was a body of revolution. The dimensions of the basic model are presented in table 1. The wing surface was not polished and no transition strip was used during these tests. The wing was tested with spoilers, with heights of 8.33 percent chord and 4.16 percent chord, which were of sufficient height to achieve a change in the wing flow conditions, especially the boundary layer, and not for the purpose of obtaining airfoil performance. They are called spoilers herein in the sense that they spoiled the airflow even though, when located on the lower surface of the wing, they might increase the lift. The spoilers were fabricated from a standard extruded angle. The spoilers were made in 1.07-m (3.5-ft) lengths so that they could be used as either full-span or semispan spoilers. The spoiler locations were about 25 and 80 percent chord from the wing leading edge as shown in figures 3(a) and 3(b). The spoilers could be put in any of the four positions shown, and these positions are designated by Roman numerals I to IV. In addition to the full-span and semispan spoilers a spoiler 8.33 percent chord high and 15.2 cm (6 in.) long was installed at the tip along the 80-percent-chord location on either the upper or lower surfaces.

In addition to the spoilers, a wind sock, a solid cone, and a vane were placed in the tip-vortex core at various distances downstream of the wing tip (see figs. 3(c), 3(d), and 3(e) for the dimensions).

Tuft Grid and Photographic System

A 0.91- by 1.37-m $\left(3\text{- by } 4\frac{1}{2}\text{-ft}\right)$ tuft grid was mounted on the survey carriage in the full-scale tunnel to survey the tip vortex. The individual tufts, 7.62 cm (3.0 in.) long, were mounted on a 2.54-cm (1-in.) grid spacing. The tuft grid was moved laterally and vertically in an attempt to keep the vortex in the center of the tuft grid. Therefore, the tuft-grid photographs presented herein should not be used to determine relative core position. A sequence camera, for permanent recording on film of the tuft-grid pattern, was mounted in the exit cone of the wind tunnel. The camera was positioned behind the semispan-wing-tip streamline when the wing was at 0° angle of attack in order to minimize individual tuft parallax effects. A sketch of the photographic setup is shown in figure 2. A remote-control zoom-lens television camera was mounted behind a viewing window and below the tunnel exit cone. The television camera gave a continuous monitoring capability and a direct instantaneous and enlarged view of the results seen by the still camera.

Test Program

Photographs of the tuft grid were taken at each model test angle of attack with the grid located at 1, 5, 9, and 14 chord lengths downstream from the trailing edge of the semispan wing. For some special cases photographs were made at intermediate chord lengths downstream. At least two photographs were taken at each position. Whenever the vortex motion was unsteady, additional photographs were taken. The vortex core diameter was estimated from the tuft-grid photographs. For purposes of Reynolds number evaluation, the basic semispan-wing model was tested at four tunnel speeds, namely, 17.9, 25.6, 32.0, and 40.3 m/sec (58.7, 84.0, 105.0, and 132.0 ft/sec).

The motion pictures of the smoke tests were made for tunnel speeds of less than 6.1 m/sec (20 ft/sec). At higher tunnel speeds the smoke dispersed so rapidly that little useful information could be obtained.

The remaining tests with spoilers were run at the same tunnel speed, namely, at 40.3 m/sec (132.0 ft/sec). This speed corresponds to a wing Reynolds number of about 1.7×10^6 which, by applying the tunnel turbulence factor of 1.1, results in an effective Reynolds number of about 1.9×10^6. The model angle-of-attack variations were from -7° to 21°.

The semispan-wing lift and drag forces were measured with the existing external scale balance system in order to afford an aerodynamic definition of the test conditions. Twenty force data points were taken and these values were averaged at each test point.

Interpretation of Tuft-Grid Data

The data used to determine the diameter of the vortex core were taken from photographs of the tuft grid. By assuming that in the flow field outside of the vortex core region the axial velocity (parallel to the core axis) is near free-stream velocity, that the radial velocity (in or out of the core) is small, and that the gravity effects on the tufts can be eliminated by averaging, it can be shown that the tuft length, as seen on the tuft-grid photographs, is directly related to the tangential velocity around the core. The inner core region consists of a rotational fluid that has vorticity. Therefore, a vorticity meter or tuft placed inside of the vortex core will rotate or spin with the fluid. A tuft exposed to vorticity will appear as a blur on the tuft-grid photographs because of fairly high spin rate of the tuft compared to the exposure speed of the photographs. Since vorticity is a vector quantity, it can cause the tufts to rotate about a particular axis, and the axis of rotation can be other than the core axis (for example, with wing separation).

Conventionally, the vortex core diameter is defined as the distance separating the points of greatest tangential velocity measured on a line crossing the center of the vortex. However, as with other instrumentation, there are numerous difficulties in measuring this diameter precisely with a tuft grid, for example, the unsteadiness of the vortex and the finite size of the instrumentation pickup. Further, some of the tuft-grid photographs indicate a noncircular core. Also, wing separation, resulting from stall or spoilers, seems to create on the tuft grid a vorticity in a plane perpendicular to the vortex core axis.

For the clean wing operating below stall, the vortex core is fairly well defined. For these conditions the following procedure was developed to measure the vortex core diameter from the tuft-grid photographs. The blurred area, corresponding to the vorticity of the core, was first located. Just outside of this blurred area, the tufts of a small area were examined to determine which tuft was the longest. Looking diagonally across the blurred area, a corresponding longest tuft was located. With a pair of dividers, the diameter of the vortex core was measured as being the greatest distance separating the chosen tufts. This measurement was then checked by placing the set dividers across the blurred area along a diameter which was angularly displaced from the first measurement. The longest tufts were once again determined. The agreement or disagreement was noted and the checking process was repeated at least twice more for other angular positions. Thus, the core-diameter readings were averaged. With a

minimum of four measurements for each photograph, it is believed that the individual core diameter may be read to within ±1.27 cm (±1/2 in.).

DISCUSSION OF RESULTS

The discussion is presented in three sections entitled "Force Data," "Tip-Vortex Characteristics," and "Reynolds Number Effects." The discussion of force data gives the aerodynamic test conditions and the effects of the spoiler configurations. The discussion of tip-vortex characteristics includes the effect of various aerodynamic and geometric parameters on the core size as defined for this study. The discussion of Reynolds number effects provides a method for comparing the experimental data of various investigations.

Force Data

The force data for the basic wing operating at different Reynolds number are presented in figure 4. No corrections were made for airstream misalinement. The data of figure 4 indicate that the maximum lift coefficient increases with increasing Reynolds number over the entire test range. Also, below the stall, there is very little change in the drag coefficient with variations in Reynolds number.

Figures 5(a) and 5(b) present the variation in lift and drag coefficients with angle of attack for the 8.33-percent-chord-high spoiler configurations. These figures indicate the characteristics of the full-span and semispan spoilers when placed on the outboard and inboard half of the wing. Also shown are the characteristics of the 15.2-cm-(6-in-) long wing-tip spoiler. This spoiler had very little effect on the lift and drag compared with the clean wing. Figure 6 shows the lift and drag coefficients for the 4.16-percent-chord-high full-span spoiler when placed at the four different positions on the semispan wing.

Tip-Vortex Characteristics

Concern about the tip vortex generally centers about the magnitude of the tangential velocity since, presumably, the tangential velocity is largely responsible for the problems associated with tip-vortex strike on a helicopter rotor blade or for the problem of the upset of one airplane by the trailing vortex from another. It has generally been supposed that the maximum tangential velocity, and consequently the influence of the tip vortex, would be decreased if the size of the vortex core were increased; for this reason, considerable effort has been devoted to trying to establish the mechanism and controlling factors of the vortex core. The results of the present investigation are therefore discussed mainly in terms of vortex core size, maximum tangential velocity, and the factors

that affect these parameters. The results are presented mainly in the form of photographs of the tuft grid, but smoke-flow tests were made for some conditions and film from these tests is available as a film supplement (L-1113) to this paper. A request card and a description of the film will be found in the back of the paper.

Clean wing.- For the clean wing operating at a relatively high circulation value (high C_L), but below stall, the tip-vortex core diameter is a fairly definable parameter in the tuft-grid photographs. All the tuft-grid photographs of the clean-wing configuration for the four tunnel speeds were read to determine the core diameter. In order to get a statistical sample for averaging, the same photographs were read by two individuals independently. The results were examined to determine whether any of several parameters were key variables in determining the core size. From each of the assumed parameters, a least-square-fit straight line was determined. A straight line through the data may not be the correct functional relationship. For example, it is known that for zero lift there is zero circulation and zero core size and, therefore, the straight line must pass through the point $C_L = 0$ and $D_c/c = 0$. The least-square-fit straight line obtained herein does not pass through this point. A least-square-fit approach was used because of the scatter in reading the core diameter. This approach tends to minimize the error by combining the data points, such that the average value has less error than the individual data points. A statistical linear-regression-analysis method, described in reference 4, was used to determine the variance between the least-square-fit straight line and the measured data. This statistical analysis is used to determine the deviation between the individual data points and the least-square-fit straight line. This deviation is measured by the value of the correlation coefficient. Each assumed parameter was evaluated to determine whether any one parameter was a key variable.

In evaluating the core size, four parameters were investigated: (1) core diameter as a function of lift coefficient, (2) core area as a function of lift coefficient, (3) core diameter as a function of induced drag $C_L{}^2$, and (4) core area as a function of induced drag. A sample plot of the results for a Reynolds number of 1.9×10^6 and for the four assumed parameters is shown in figure 7. The data for the two individual readers are shown superimposed on the same plot. A summary tabulation of the statistical results and the least-square-fit line for the four assumed parameters and four Reynolds numbers is shown in table 2.

From the data in table 2 other functional relationships can be examined. For example, for an elliptical spanwise load distribution

$$\frac{L}{\pi b/4} = \frac{\frac{1}{2}\rho V^2 S C_L}{\pi b/4} = \rho V \Gamma$$

therefore,

$$C_L = \frac{\pi b}{2} \frac{\Gamma}{SV}$$

Substituting this value of C_L into $\frac{D_c}{c} = A + BC_L$ from table 2 results in

$$\frac{D_c}{c} = A + \left(\frac{\pi b}{2SV}\right)B\Gamma$$

Therefore, the parametric relationship $\frac{D_c}{c} = A + E\Gamma$ can be determined from the results in table 2 by simply changing the slope parameter B in table 2 $\left(\text{i.e., } E = \left(\frac{\pi b}{2SV}\right)B\right)$.

Table 2 includes a parameter r^2, the correlation coefficient squared. The square of the correlation coefficient may be interpreted quantitatively as equal to the variance of the core size $\frac{D_c}{c}$ or $\left(\frac{D_c}{c}\right)^2$ that has been accounted for by the relationship with C_L or $C_L{}^2$. For example, if the correlation coefficient is 0.80 ($r = 0.80$), then 64 percent $\left(r^2 = 0.64\right)$ of the variance of D_c or $D_c{}^2$ could be explained by the assumed functional relationship between core size and lift coefficient. A correlation coefficient of 1.0 means that the experimental data do not deviate from the least-square-fit line, that is, all the data fall in a straight line. Of course, scatter in the experimental data is reflected in the magnitude of the correlation coefficient. In other words, the assumed functional relationship cannot fit the data well if there is a lot of scatter in the data, and this scatter will result in a lower correlation coefficient.

By referring to table 2 and considering any one functional relationship $\left(\text{e.g., } \frac{D_c}{c} = A + BC_L\right)$ for the four Reynolds numbers, it is seen that the lowest Reynolds number has a very small correlation coefficient $\left(r^2 = 0.28\right)$. This implies that the assumed functional relationship was a poor choice and there must be other variables that are important (e.g., drag coefficient). For the three highest Reynolds numbers about three-fourths of the variance $\left(r^2 = 0.75\right)$ in core size can be attributed to the assumed functional relationship. However, a comparison of the correlation coefficient for any one Reynolds number and all four functional relationships indicates that no one single functional relationship is superior to another. It is concluded from this that the assumed functional relationships are not the exact ones (e.g., the core size does not go to zero with the lift coefficient). Further, there seems to be a relatively strong relation between the core size and lift coefficient for the three highest Reynolds numbers and a weak relationship for the lowest Reynolds number.

In addition to the linear regression analysis using the variables C_L and $C_L{}^2$, a multiple linear regression analysis using C_L, $C_L{}^2$, and C_D was attempted. For

example, a functional relationship was assumed as follows: $\frac{D_c}{c} = A + BC_L + CC_D + EC_L^2$ where A, B, C, and E are constant coefficients. The resulting correlation coefficient did not increase significantly above those presented in table 2. This is believed to be due to the scatter in the data.

The smoke-flow tests provided some information on the axial velocities in the vortex core. The smoke tests were made at tunnel speeds between about 6.1 m/sec (20 ft/sec) and 4.5 m/sec (15 ft/sec). At higher speeds the smoke dispersed too rapidly to provide valuable information. Because of the mass of the smoke particles, centrifugal force concentrates the smoke in the vortex core at its outer periphery; thus, the core behavior can be visualized on the film. By using intermittent smoke emission, axial velocities above or below free-stream velocity can be visualized. The film indicates that initially the core axial-velocity component is greater than free stream and that farther downstream it becomes less than free stream. This result is in agreement with the results presented in reference 5.

Wing with spoilers.- Reference 1 states that the wing boundary layer forms the vortex sheet that ultimately rolls up into the core. This seems to be a logical statement since the wing frictional losses and vorticity originate within the boundary layer and are shed in a trailing vortex sheet. Downstream this same vorticity has been shown to roll up into the vortex core. Therefore, it seems logical to assume that the downstream fluid-momentum losses, due to profile drag, would appear within the tip-vortex core and thus, the thicker the wing boundary layer, the larger the downstream core size would be. Reference 6 states that a small vertical panel (or spoiler) mounted on the upper wing surface produced a significant reduction in the maximum tangential velocity in the trailing vortex. The statements in both of these references seem logical and consistent in that a small vertical panel on the wing upper surface would be expected to increase the boundary-layer thickness and this, in turn, might be expected to increase the core size, which for a constant circulation, or lift, would decrease the maximum tangential velocity around the vortex core. In order to explore this phenomenon further, a number of spoiler configurations were investigated in the present program.

Figures 8 and 9 are photographs of the tuft grid showing the wing tip vortex for various spoiler configurations with the tuft grid at 5 chord lengths downstream of the wing trailing edge. The figures are for an effective Reynolds number of about 1.9×10^6. Figures 8 and 9 are for near-constant lift coefficients of 0.9 and 1.0, respectively, and for markedly different drag coefficients depending on the spoiler configuration. These figures show that the vortex core is much less well defined when the spoilers are installed than for the clean wing. It seems, from inspection of the figures, that the intensity of the vorticity in the core is reduced by the spoilers but the general level of

turbulence in the vicinity of the core is increased. This increase in turbulence is probably associated with the separated flow behind the spoiler. (Note that the wing was not stalled and was operating at only about two-thirds of its maximum lift coefficient, as indicated by figs. 5 and 6.) This turbulence was of a different character from the vorticity in the vortex core in that a high percentage of the tuft activity was observed to be in the plane of the tuft grid rather than along the core axis as was the case for the clean wing. The turbulence is not well understood and has an odd pattern in that there is less turbulence in the vicinity of the tip-vortex core when there is no spoiler at the wing tip, as would be expected, but there is more turbulence for the case of the tip spoiler than for the case of the full-span spoiler.

Because of the doubt as to how to interpret the photographs, as a result of the general turbulence in the vicinity of the tip-vortex core, no positive indication of the effects of the spoilers on the core size can be obtained. It can be determined, however, from estimates of the tangential velocity from the tuft grid, that there is no significant effect of the spoilers on the maximum tangential velocity. This result, together with the previously noted fact that the spoilers reduced the intensity of the vorticity in the core, seems to be contrary to statements of references 1 and 6. These references would seem to indicate that the spoilers, which cause an increase in drag, would cause an increase in the amount of boundary layer which would roll up into the tip-vortex core with a resultant increase in core size and a consequent reduction in maximum tangential velocity. One possible explanation for these differences is the difference in Reynolds number. The data in reference 1 were obtained at a Reynolds number of about 0.25×10^6, whereas the Reynolds number for the tests reported herein was about 1.9×10^6. The results of the full-scale flight tests reported in reference 6 were inconclusive.

In an attempt to answer the question of whether all the wing boundary layer goes into the vortex core, photographs of smoke emitted upstream of the wing leading edge were taken at three spanwise locations. These photographs, presented as figure 10, indicate that only the smoke emitted at the wing tip goes into the wing tip vortex. The film supplement also indicates that all the boundary-layer fluid does not end up in the tip-vortex core, at least for the downstream-distance limits of these tests. It appears rather that the boundary-layer fluid subjected to three-dimensional effects near the tip tends to form the vortex core. Smoke emitted at 50 and 75 percent span was slightly affected by the tip vortex. The outer 10 percent of the span seemed to have the largest effect on the tip-vortex formation. Because of difficulties in evaluating smoke flow, these conclusions can only be considered to be tentative. For example, even though attempts were made to keep the smoke within the boundary layer, the density of the boundary-layer smoke may have been such that it was not as visible as the smoke not in the boundary layer.

In addition to the full-span and semispan spoilers, a smaller 15.2-cm- (6-in-) long spoiler was also tested. For these tests, the spoiler was placed at the tip of the wing along the 80-percent-chord location and was tested on both the upper and lower surfaces of the wing. Figures 11 and 12 are photographs of the tuft grid showing the tip vortex for this short (15.2-cm (6-in.)) spoiler at wing angles of attack of 16.8° and 18.8°, respectively, and for a Reynolds number of about 1.9×10^6. A comparison of lift coefficient for these spoiler configurations and the clean wing (fig. 5) indicate no significant differences. Figures 11 and 12 indicate that the vorticity as determined by the blurred tufts has been decreased and the core size seems to be smaller for the modified wings than for the clean wing. However, the core size, as determined from the maximum tangential velocity, seems to be about the same for all three configurations. Estimates of the maximum tangential velocity from the tuft photographs for the three configurations are about the same magnitude. There seems to be slightly more turbulence in the flow field outside of the core (potential field) for the two spoiler configurations than for the clean wing.

It is concluded from the foregoing tests that at full-scale Reynolds number and at the same lift or lift coefficient, the spoiler configurations tested tended to decrease the vorticity within the vortex core and made no significant change in the maximum tangential velocity. This conclusion is based on comparison with results for the clean wing.

Trailing objects in core.- In addition to the foregoing basic program some exploratory investigations were performed. An attempt was made to affect the vortex core with some wing-tip trailing objects.

First, the wind sock shown in figure 3(c) was "played out" (from 1 to 3 chord lengths) on a wire trailing from the wing tip. The thought was to capture the core within the wind sock, create a downstream pressure gradient within the wind sock, and bring on the onset of vortex bursting. Recall that vortex bursting has been associated with an adverse pressure gradient (ref. 7). This test resulted in the wind sock rotating in a large circular path away from the vortex core area. A restraint wire was then placed in the trailing position downstream of the wind sock, such that there were now two streamwise restraint wires, forward and aft of the wind sock. The tuft grid and television monitor were used to guide the wind sock into the vortex core position. This setup resulted in the wind sock rotating about its own axis (as a rigid body in the vortex core) until it twisted the restraint wires and broke some wire strands and eventually the wind sock became torn. The wind sock seemed to disperse the vortex core, but the result was inconclusive because of the short duration of the test.

An exploratory attempt to disturb the vortex was also made by placing the solid cone shown in figure 3(d) in the vortex core. The cone was fixed to a long boom which was in turn fixed to the tuft grid with the cone located 4 chord lengths ahead of the tuft

grid. By monitoring the tuft grid on the zoom-lens television camera, the cone could be placed in the vortex core. Figure 13 presents photographs of the tuft grid with the cone above (fig. 13(a)) and inside (fig. 13(b)) the tip-vortex core. The photographs indicate that the vorticity in the core, as shown by the blurring of the tufts, is decreased when the cone is in the core. However, the core size as determined from the maximum tangential velocity is also about the same as for the clean wing. The decrease in vorticity is probably due to the separation that exists at the trailing edge of the cone body. Similar results were obtained with the tuft grid at 10 chord lengths downstream and at other wing angles of attack. These cone tests were duplicated at lower tunnel speeds by using a smoke generator to show visually that the cone did tend to eliminate the central core region. The results are shown in the film supplement mentioned previously.

A small 10.1- by 20.3-cm (4- by 8-in.) vane (which is about 1.5 percent of the area of the wing semispan) shown in figure 3(e) was attached to the wing tip approximately 1/2 chord length downstream of the wing trailing edge. The effect of the vane is shown by the tuft-grid photographs of figures 14(a) and 14(b) and by the smoke-flow tests in the film supplement. The figures indicate that the vorticity, as determined from the blurring of the tufts, is greatly reduced by the vane. Inspection of the tuft-grid photographs indicated that the core size, as determined from the maximum tangential velocity (tuft length), is about the same for all these photographs, but the maximum tangential velocity is decreased by the vane. Since reduction in the tangential velocity is a particular goal, the tangential velocities were determined for the clean wing with and without the vane, and the data are presented in figure 14(c). The scatter in the data results from the inability to read the tuft lengths precisely, but there seems to be no doubt that the maximum tangential velocity is reduced by use of the vane. At radial distances beyond about 0.25c $\left(D_c/c = 0.5\right)$, however, there is no clear-cut effect of the vane.

There is a question as to whether the vane simply disorganized the core without really eliminating the vorticity, with the possibility that the core would become reorganized farther downstream. Tuft-grid photographs made at distances of 9 and 14 chords downstream are presented in figures 14(d) and 14(e). These data were taken at a higher Reynolds number than those of figures 14(a) and 14(b) but are believed to be comparable. In any event, figures 14(d) and 14(e) show that there is no evident increase in vorticity within the core as compared with the photographs of figure 14(b) taken at a distance of 5 chords.

Reynolds Number Effects

Reynolds number effects on the tip vortex are evaluated in this section on a basis of vortex core size. The flow region outside of the vortex core is generally accepted as being a potential flow region and would therefore be expected to be unaffected by viscous

forces. The tip-vortex inner core region consists of fluid in a rotational state which does not permit a potential flow solution. Therefore, it is this inner core region that might be expected to be most subjected to viscous forces. Reynolds number, which reflects scale effects, is the ratio of fluid inertia to fluid viscous forces. It is expected that where the viscous forces exist, namely, in the inner core region, the Reynolds number effects should be most pronounced.

Taking any one of the functional relationships in table 2 and comparing this for the four Reynolds numbers indicate that the least-square-fit lines are nearly the same for the three highest Reynolds numbers, but that they are markedly different for the lowest. Further, for the lowest Reynolds number, the tip-vortex core size increases at a slower rate (lower curve slope) than for the higher numbers. For example, take the relationship $D_c = A + BC_L$; for the four Reynolds numbers, from the lowest to the highest, $A = 0.0692$, 0.0338, 0.0512, and 0.0562 and $B = 0.0521$, 0.1438, 0.1404, and 0.1258, respectively. Note that the slope B for the three highest Reynolds numbers is approximately the same and also that this slope is approximately $2\frac{1}{2}$ times the slope for the lowest Reynolds number. This trend is also shown graphically in figure 15. This same characteristic is true for any of the four parametric relationships shown in table 2. Thus, it is concluded that a Reynolds number effect on the tip-vortex core size does exist and that the critical value of Reynolds number above which there is little further effect is between 0.8×10^6 and 1.2×10^6.

A pictorial method of viewing the Reynolds number effects is to view the tip-vortex photographs for the different dynamic pressures with various parameters held constant. For example, photographs of the tip vortex for the four dynamic pressures are shown in figures 16 and 17 for a near-constant lift force of 289 N (65 lb) and 178 N (40 lb), respectively; in figures 18 and 19 for a near-constant circulation of 2.79 m^2/sec (30 ft^2/sec) and 4.83 m^2/sec (52 ft^2/sec), respectively; and in figures 20 and 21 for a near-constant lift coefficient of 0.91 and 1.04, respectively. Figures 16 and 17 are for a near-constant lift force, and hence the circulation decreases with increasing dynamic pressure, as would be expected, since for an elliptical loading $\Gamma = \frac{L}{\pi b/4} \frac{1}{\rho V}$. Also, for a constant lift force the core size appears to decrease with increasing dynamic pressure or decreasing lift coefficient (same as the results in table 2). In figures 18 and 19, for near-constant circulation and varying dynamic pressure, it appears that the core size is constant for the four dynamic pressures and, therefore, is independent of dynamic pressure. However, the results of the larger data sample in the statistical analysis in table 2 discounts this conclusion. The results in figures 20 and 21 show more clearly the results presented in table 2; namely, for the three highest dynamic pressures, the

core size is nearly the same for a given lift coefficient, whereas it is significantly smaller for the lowest dynamic pressure.

An attempt was made to evaluate the Reynolds number effects with the use of a vorticity meter. Photographs of the meter and its installation are shown in figure 22. In using the meter numerous difficulties were encountered in keeping the meter properly lubricated. Pretest and post-test calibrations were inconsistent. In addition, in traversing the vortex core area with the meter, the vanes would sometimes oscillate rather than rotate, and when the vanes were alined properly with the photocell in the meter, this oscillation would result in a pulse similar to that of the rotating vane. This difficulty was overcome by closely observing the vorticity meter vanes while making meter readings. Further, the conversion factor for converting the vane rotational speed to vorticity apparently was not constant because of the inability to compute the wing lift consistently (as measured on the wind-tunnel scales) from the rotational speed of the vorticity meter. Hence, no Reynolds number evaluation was made based on the vorticity-meter results; however, a typical rotational speed map obtained with the vorticity meter is presented in figure 23. The results are similar to those obtained by other investigators. The results indicate that the vorticity rolls up rapidly (within 1 or 2 chord lengths downstream) and, further, that the vorticity is concentrated within the core of the wing tip vortex.

CONCLUDING REMARKS

An investigation was conducted in the Langley full-scale tunnel to study some factors affecting the tip vortex of a wing. The data obtained consisted of measurement of the properties of the vortex by use of a tuft grid, measurement of the aerodynamic forces on the wing, and qualitative analysis of smoke-visualization studies.

Wind-tunnel tests were performed on a semispan wing at four tunnel speeds between 17.9 m/sec (58.7 ft/sec) and 40.3 m/sec (132.0 ft/sec) in order to determine the effects of Reynolds number on the tip-vortex core size. The results indicate that there is a definite Reynolds number effect. The tip-vortex core size seems to increase with increasing lift coefficient at nearly the same rate for the three highest Reynolds numbers, whereas for the lowest Reynolds number the core size increases with increasing lift coefficient at a much slower rate. This change in the core-size behavior occurred at a Reynolds number between 0.8×10^6 and 1.2×10^6.

An attempt was made to determine what parameters influence the tip-vortex core size. Numerous functional parameters such as lift, drag, and induced drag were chosen and correlated with the core size. The results indicate that, of the functions chosen, not

one was superior to the others. Therefore, it is concluded that the core size must either be defined with more accurate data than were obtained in this study or the core size must be defined by parameters other than those considered.

Spoilers were placed on either the upper or lower surface of the wing to increase the boundary-layer thickness and/or drag. All these tests were run at the highest tunnel speed, which corresponds to a Reynolds number of about 1.9×10^6. For the same lift the full-span spoilers seemed to decrease the vorticity within the core when compared with that of the clean wing, but the core diameter determined from the maximum tangential velocity is about the same. Since the spoilers were expected to increase the boundary-layer thickness on the wing, a resulting change in vortex core size was also expected. It appeared that this increase in boundary-layer thickness resulted in no change in the vortex core size, which seems contrary to some previously published statements. Further, the maximum tangential velocity seemed to be about the same for the clean wing and the wing with the spoilers as long as the lift coefficient remained the same. Similar tests were made with smaller full-span and partial-span spoilers and the same conclusions were reached.

Smoke tests were performed at a relatively slow tunnel speed. The smoke test confirmed the results of the spoiler tests, namely, that not all the boundary-layer fluid is transmitted to the vortex core. In particular, it appears that only the fluid that is subjected to three-dimensional effects has an influence on the tip vortex. The smoke tests also indicated that the vortex core, upon initially leaving the wing, has an excess axial velocity in the free-stream direction, but that further downstream the axial velocity of the core becomes less than the free-stream velocity.

Various solid objects were placed downstream of the wing tip in an attempt to break up the tip-vortex core and reduce the tangential velocities in the vortex. The most successful object was a small vane, attached to the wing tip, having an area of about 1.5 percent of the area of the semispan wing, whose surface was alined with the free stream approximately 1/2 chord length downstream of the wing trailing edge. The vane seems to decrease the vorticity greatly within the core and also to decrease the maximum tangential velocity. The core size, as determined from the maximum tangential velocity, is about the same as for the clean wing. These results are documented with the tuft grid and with smoke visualization.

Langley Research Center,
National Aeronautics and Space Administration,
Hampton, Va., February 18, 1972.

REFERENCES

1. McCormick, Barnes W.; Tangler, James L.; and Sherrieb, Harold E.: Structure of Trailing Vortices. J. Aircraft, vol. 5, no. 3, May-June 1968, pp. 260-267.

2. Spreiter, John R.; and Sacks, Alvin H.: The Rolling Up of the Trailing Vortex Sheet and Its Effect on the Downwash Behind Wings. J. Aeronaut. Sci., vol. 18, no. 1, Jan. 1951, pp. 21-32, 72.

3. Scheiman, James; and Shivers, James P.: Exploratory Investigation of the Structure of the Tip Vortex of a Semispan Wing for Several Wing-Tip Modifications. NASA TN D-6101, 1971.

4. Hoel, Paul G.: Introduction to Mathematical Statistics. John Wiley & Sons, Inc., c.1947.

5. Chigier, N. A.; and Corsiglia, V. R.: Tip Vortices – Velocity Distributions. Amer. Helicopter Soc. Preprint No. 522, May 1971.

6. Corsiglia, Victor R.; Jacobsen, Robert A.; and Chigier, Norman: An Experimental Investigation of Trailing Vortices Behind a Wing With a Vortex Dissipator. NASA paper presented at the Symposium on Aircraft Wake Turbulence (Seattle, Wash.), Sept. 1970.

7. Lowson, M. V.: Some Experiments With Vortex Breakdown. J. Roy. Aeronaut. Soc., vol. 68, no. 641, May 1964, pp. 343-346.

TABLE 1.- CHARACTERISTICS OF THE BASIC SEMISPAN WING AND SPOILERS

Airfoil section	NACA 0012
Chord, cm (in.)	60.96 (24)
Thickness, cm (in.)	7.31 (2.88)
Span, m (ft)	2.13 (7)
Reference area, m^2 (ft^2)	1.3 (14)
Twist, deg	0
Large spoiler height, cm (in.)	5.08 (2.0)
Small spoiler height, cm (in.)	2.54 (1.0)

TABLE 2.- SUMMARY OF STATISTICAL RESULTS

Functional relationship	A	B	r^2	q		R
				N/m^2	lb/ft^2	
$\frac{D_c}{c} = A + BC_L$	0.0692	0.0521	0.28	189.6	3.96	0.8×10^6
	.0338	.1438	.76	387.8	8.10	1.2
	.0512	.1404	.77	600.9	12.55	1.5
	.0562	.1258	.70	962.9	20.11	1.9
$\frac{D_c}{c} = A + BC_L^2$	0.0862	0.0350	0.25	189.6	3.96	0.8×10^6
	.0775	.0988	.72	387.8	8.10	1.2
	.0925	.0954	.75	600.9	12.55	1.5
	.0962	.0788	.65	962.9	20.11	1.9
$\frac{D_c^2}{c^2} = A + BC_L$	0.00422	0.0108	0.27	189.6	3.96	0.8×10^6
	-.00628	.0379	.78	387.8	8.10	1.2
	-.00500	.0430	.73	600.9	12.55	1.5
	-.00380	.0340	.78	962.9	20.11	1.9
$\frac{D_c^2}{c^2} = A + BC_L^2$	0.00769	0.00745	0.25	189.6	3.96	0.8×10^6
	.00483	.0268	.78	387.8	8.10	1.2
	.00719	.0300	.76	600.9	12.55	1.5
	.00889	.0241	.78	962.9	20.11	1.9

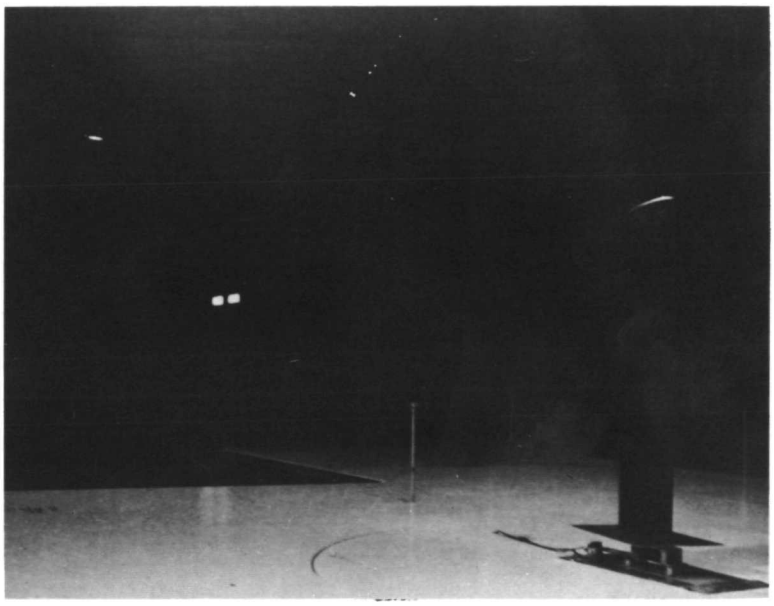

L-72-137

Figure 1.- Photograph of semispan model setup in Langley full-scale tunnel.

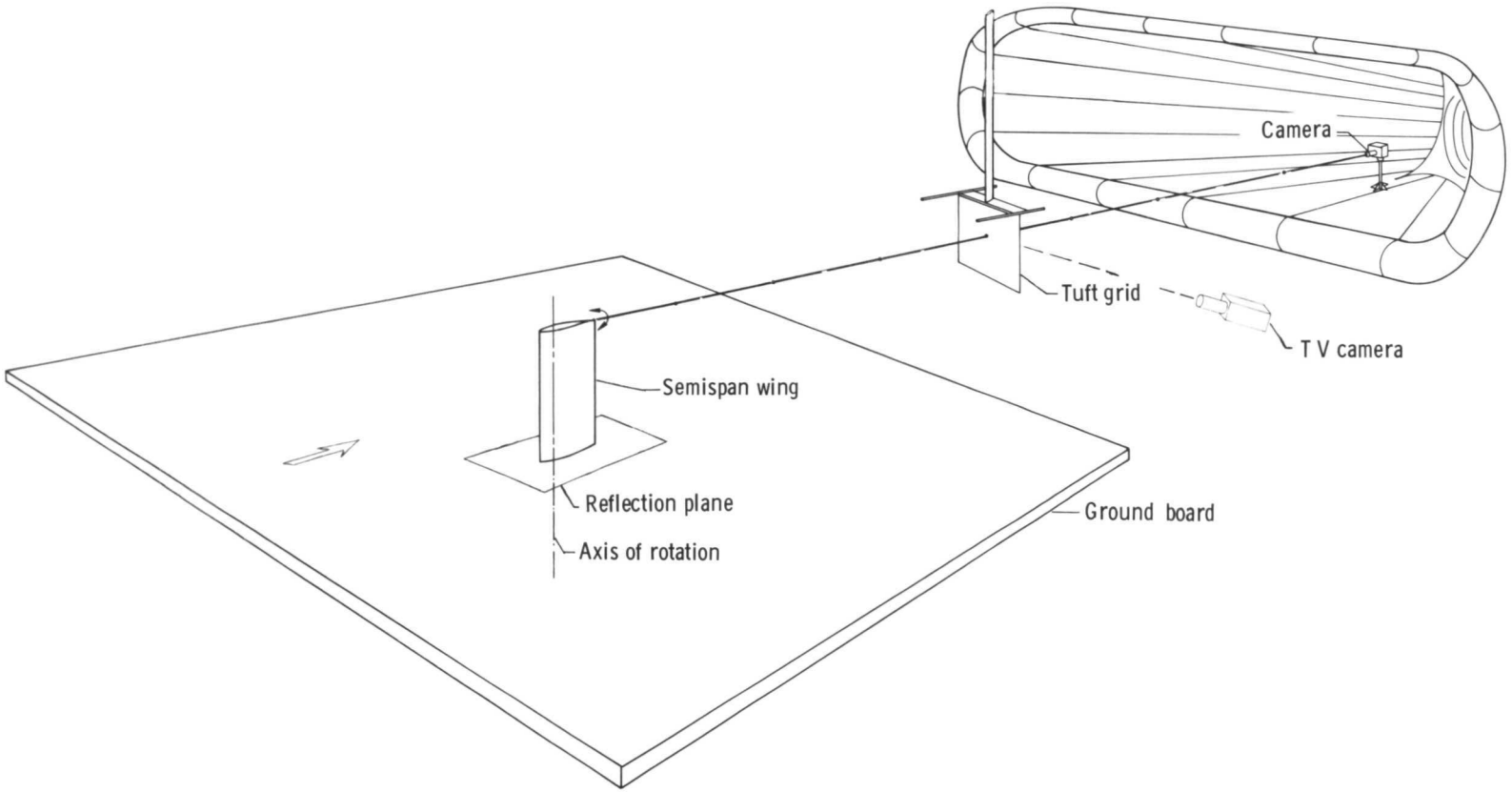

Figure 2.- Sketch of semispan-wing model, camera, and tuft grid setup in wind tunnel.

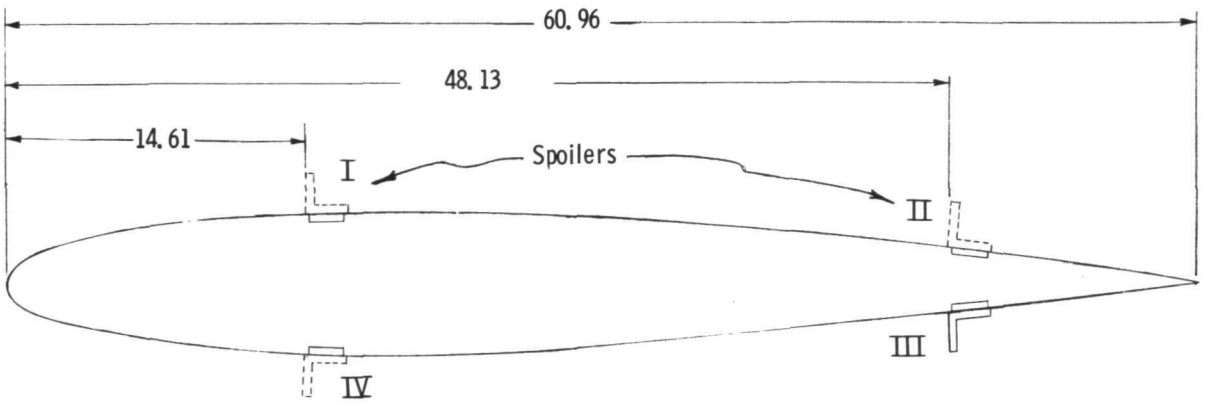

(a) Wing with 8.33-percent-chord-high spoilers.

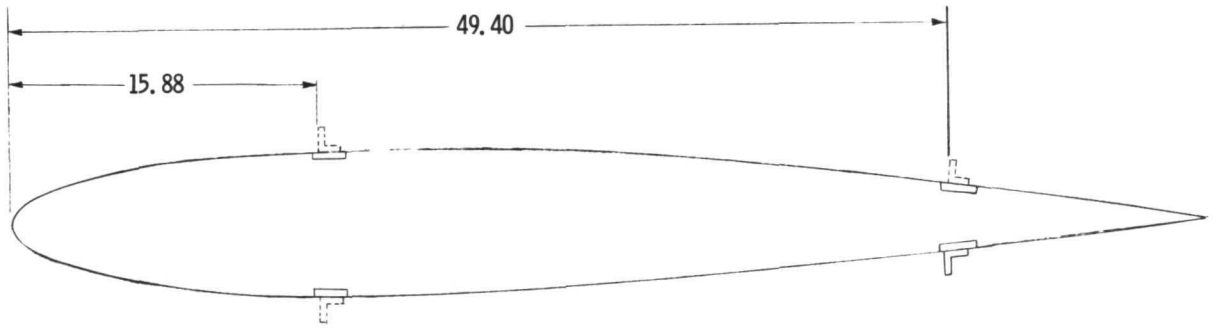

(b) Wing with 4.16-percent-chord-high spoilers.

Figure 3.- Sketch of various model configurations used to determine effectiveness of disturbing trailing tip vortex of semispan wing. All dimensions in cm unless noted.

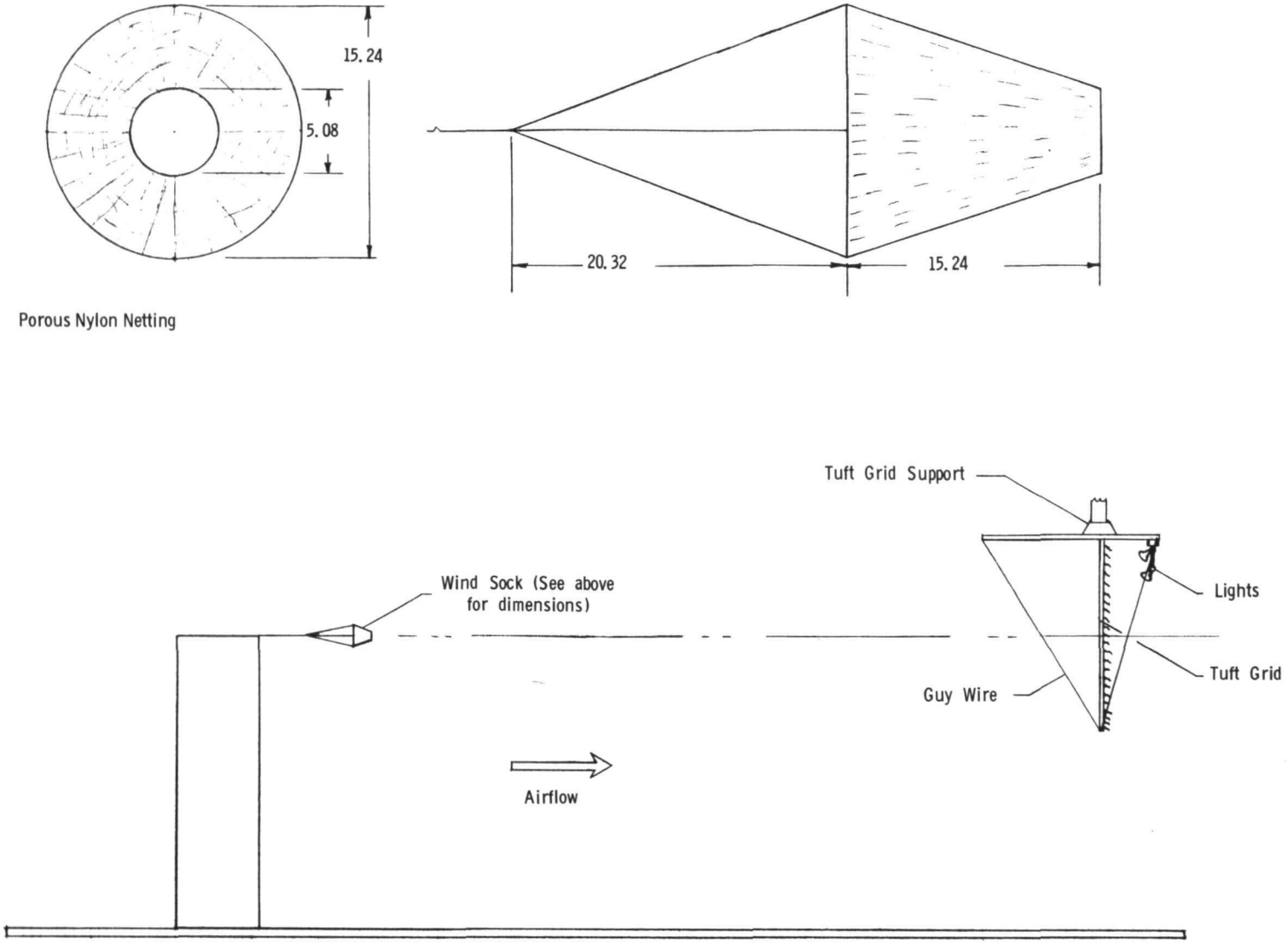

(c) Wing with wind sock.

Figure 3.- Continued.

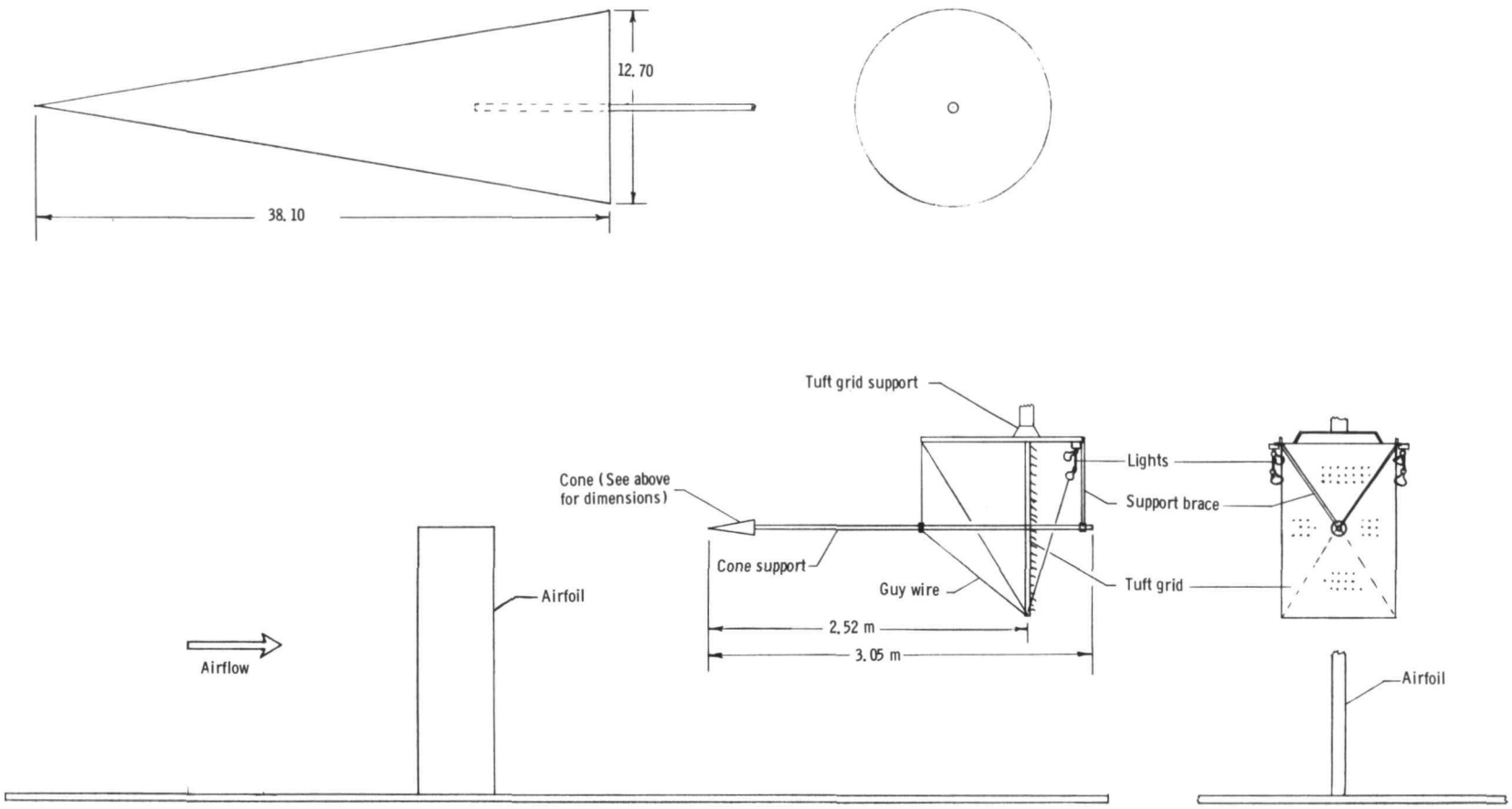

(d) Wing with solid cone.

Figure 3.- Continued.

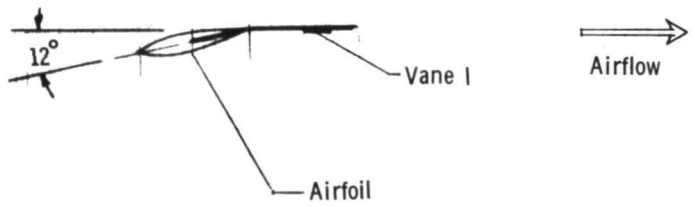

Dimensions for vanes, cm		
Vane	Width	Height
1	10.1	20.3

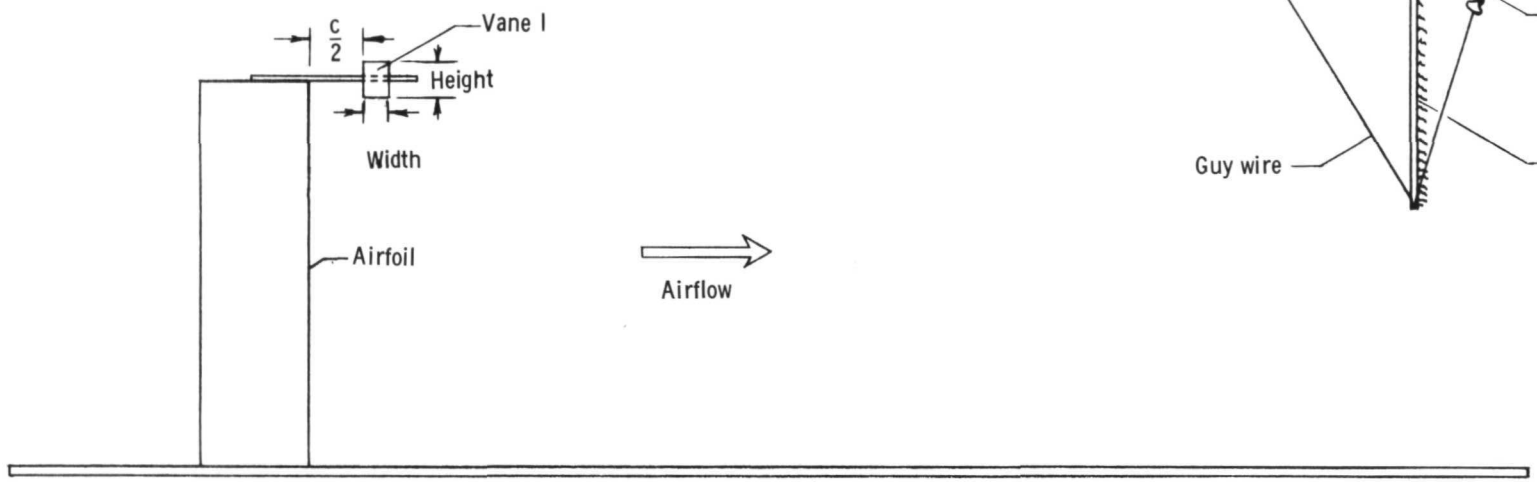

(e) Wing with vane.

Figure 3.- Concluded.

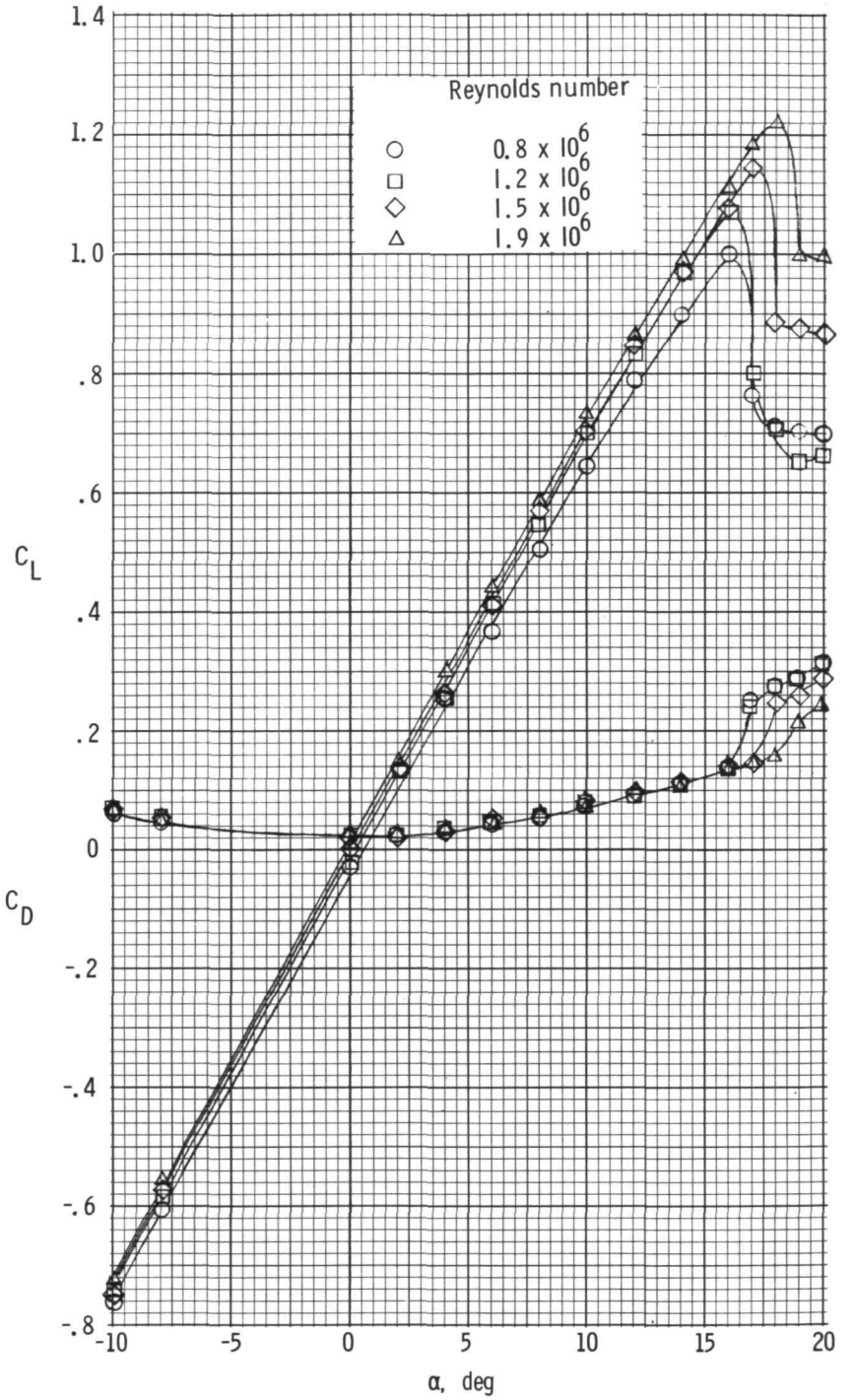

Figure 4.- Variation of lift and drag coefficients with angle of attack for various Reynolds numbers for clean wing.

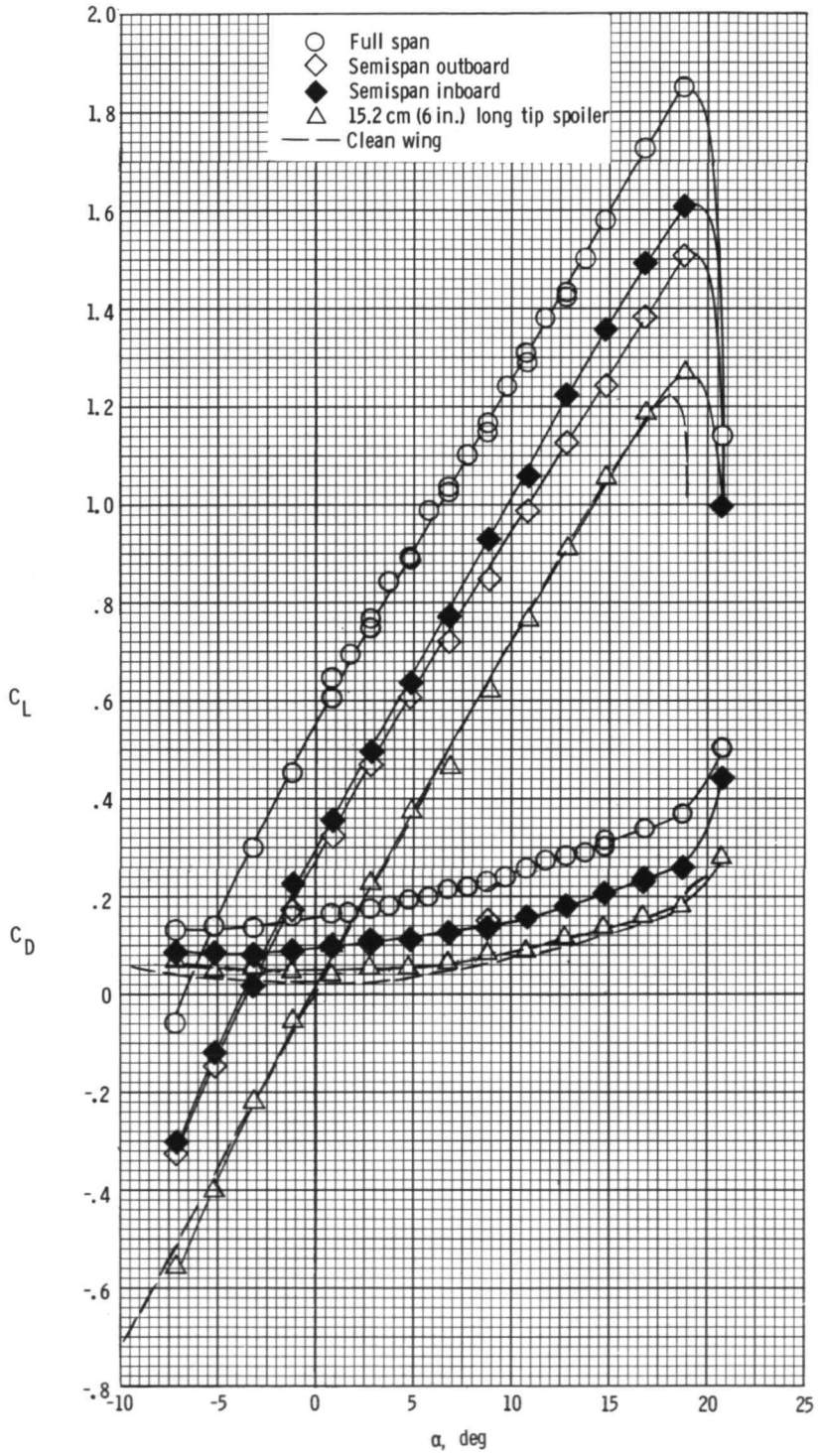

(a) Spoilers in position III.

Figure 5.- Variation of lift and drag coefficients with angle of attack for 8.33-percent-chord-high spoilers and clean wing. $R = 1.9 \times 10^6$.

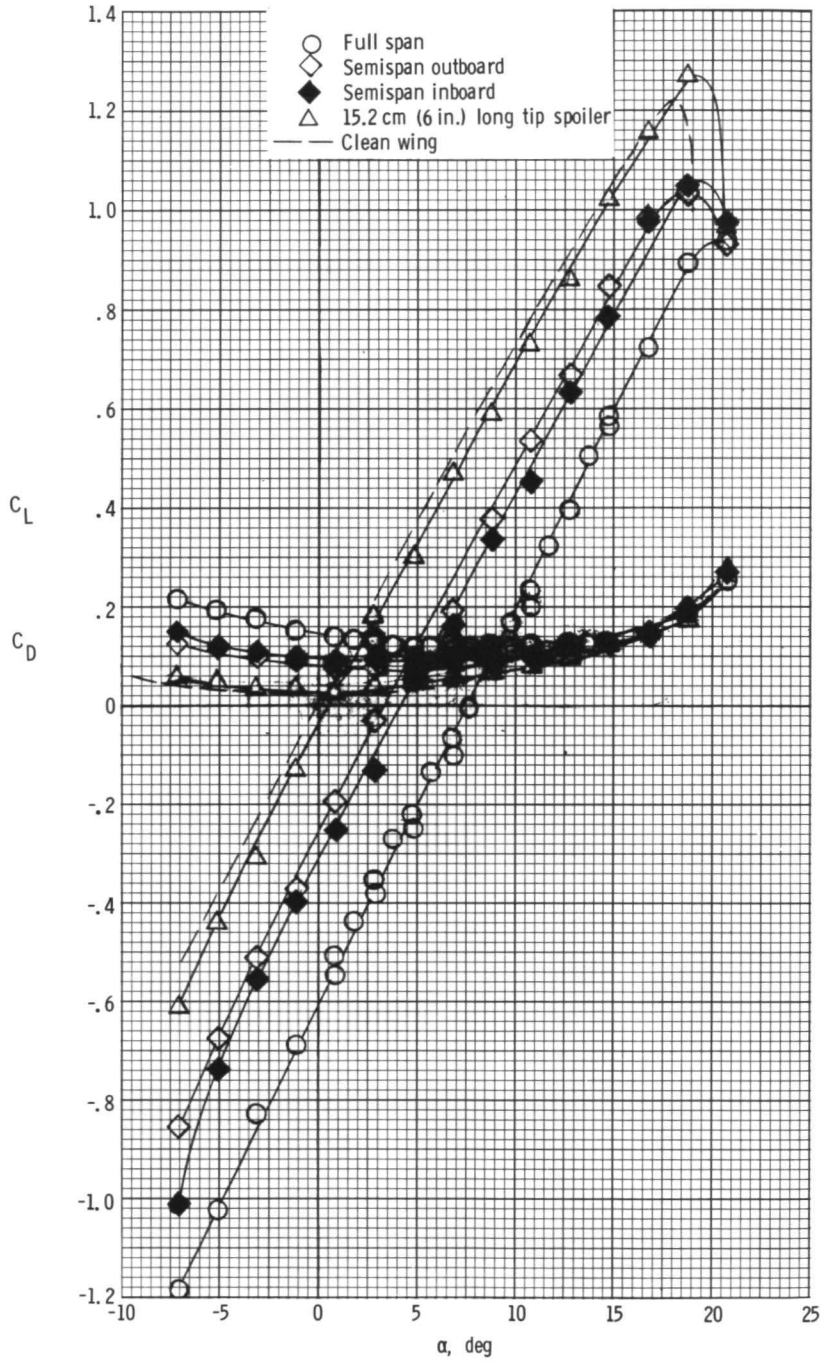

(b) Spoilers in position II.

Figure 5.- Concluded.

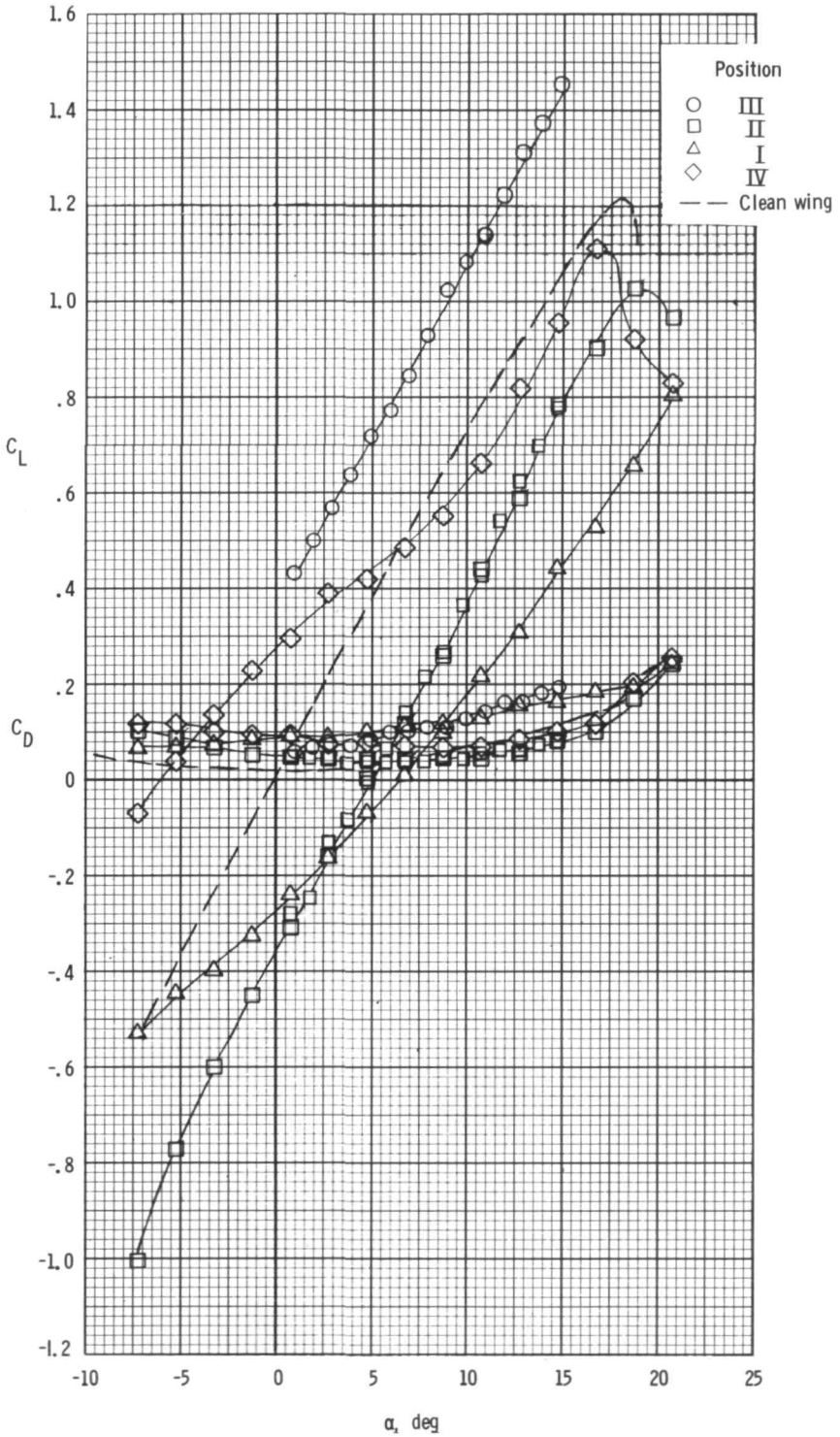

Figure 6.- Variations of lift and drag coefficients with angle of attack for full-span 4.16-percent-chord-high spoiler at various positions. $R = 1.9 \times 10^6$.

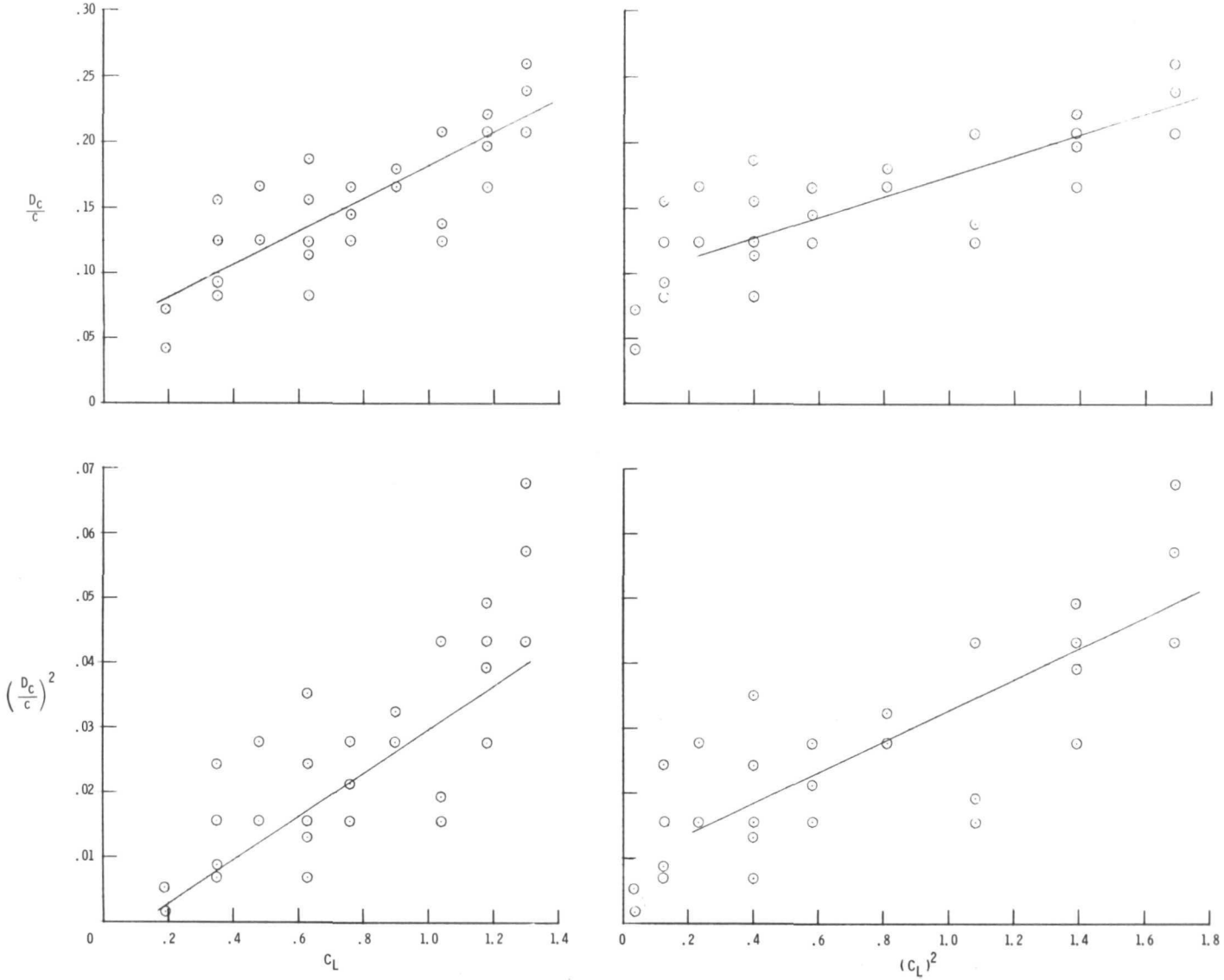

Figure 7.- Least-square-fit line for various functional relationships between D_c/c and C_L. $R = 1.9 \times 10^6$; 5 chord lengths downstream.

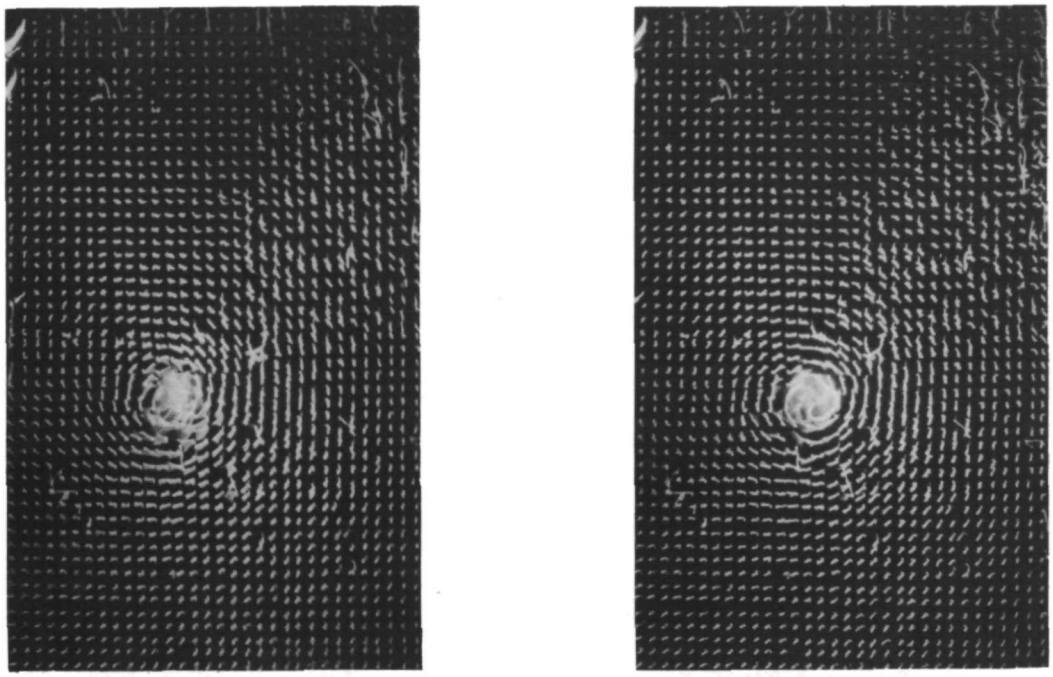

(a) Clean wing. $C_L = 0.90$; $C_D = 0.095$.

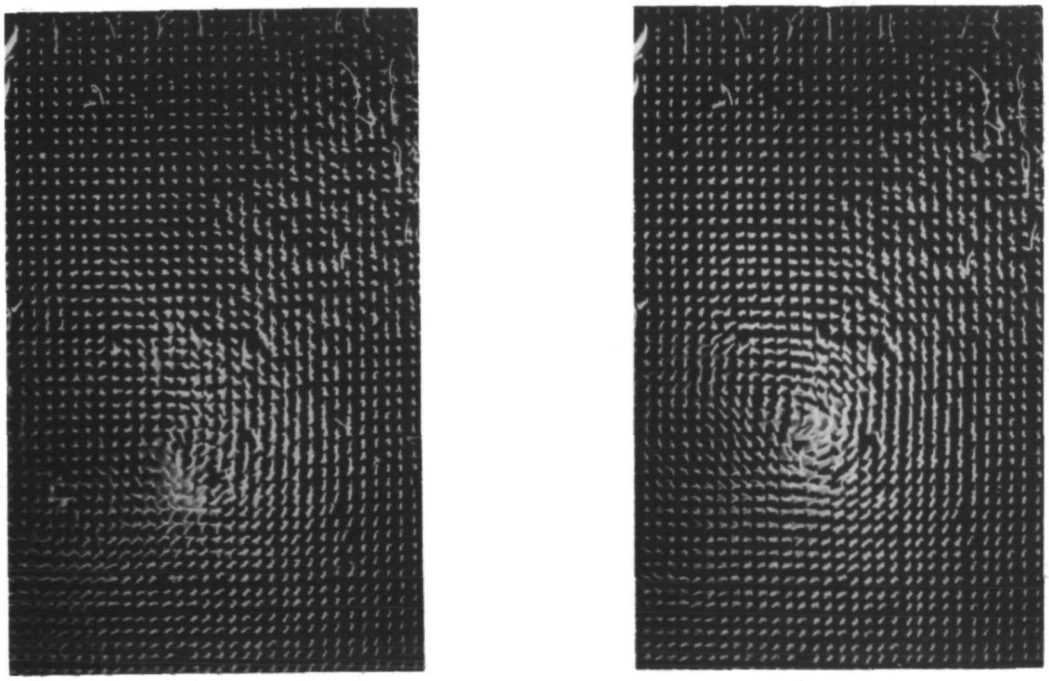

(b) 8.33-percent-chord-high full-span spoiler. $C_L = 0.90$; $C_D = 0.19$.

(c) 4.16-percent-chord-high full-span spoiler. $C_L = 0.93$; $C_D = 0.11$.

Figure 8.- Photographs showing effect of full-span and semispan spoilers on tip vortex at 5 chord lengths downstream for a near-constant lift coefficient of about 0.9. Spoiler position III; $R = 1.9 \times 10^6$.

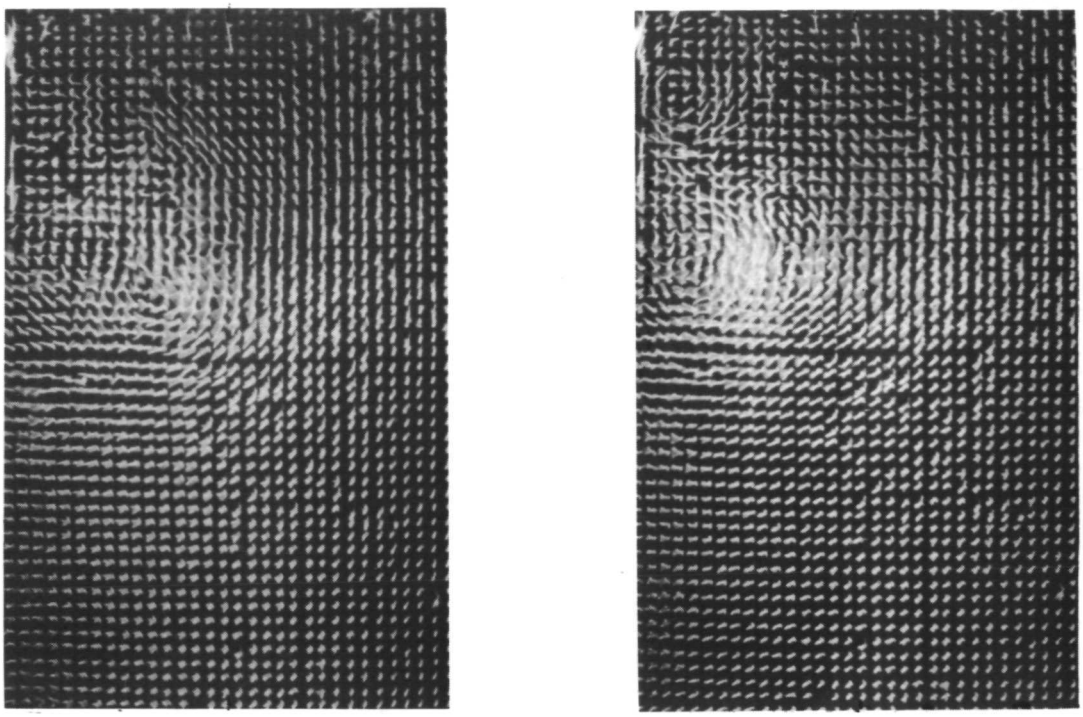

(d) 8.33-percent-chord-high spoiler on semispan outboard. $C_L = 0.92$; $C_D = 0.14$.

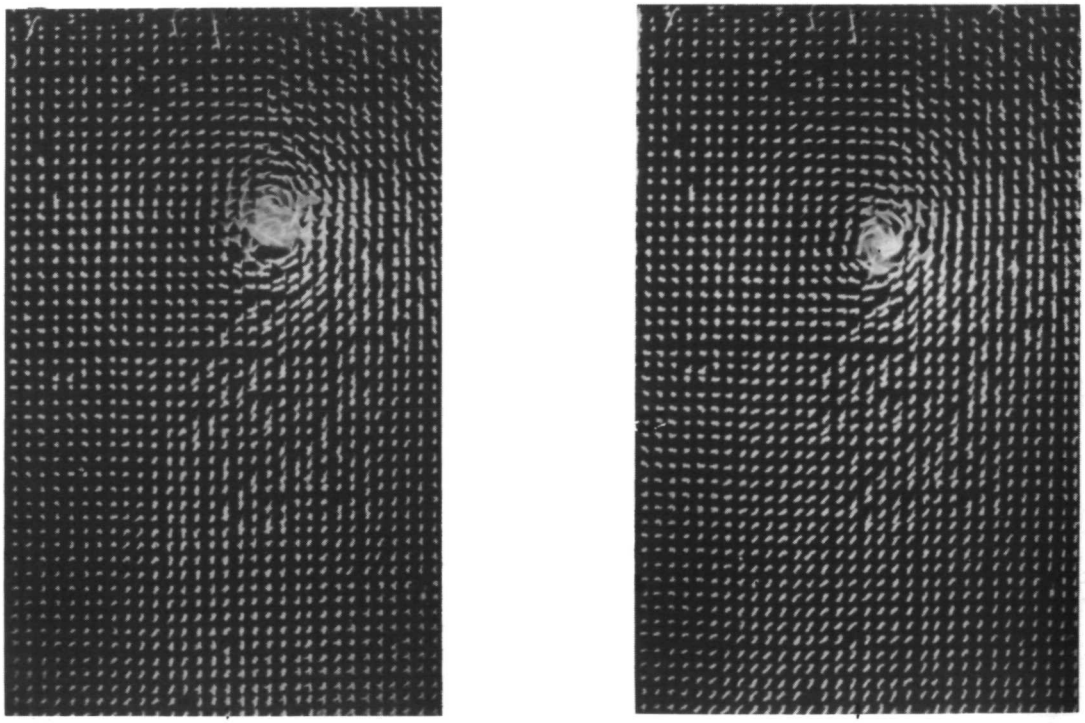

(e) 8.33-percent-chord-high spoiler on semispan inboard. $C_L = 0.85$; $C_D = 0.13$.

Figure 8.- Concluded.

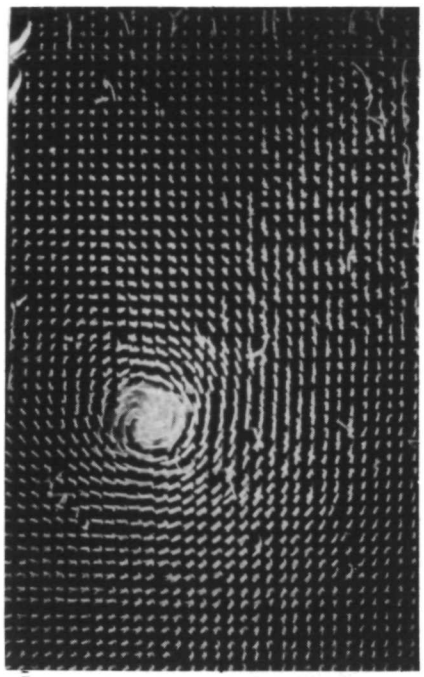

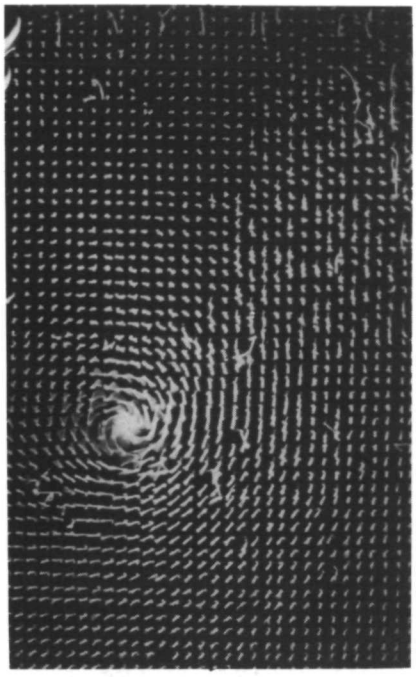

(a) Clean wing. $C_L = 1.04$; $C_D = 0.12$.

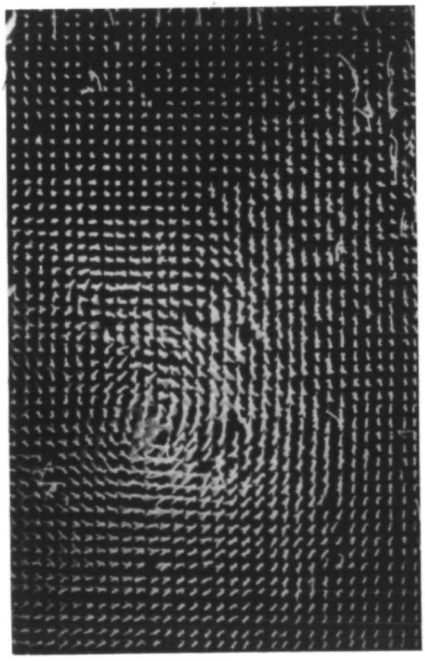

(b) 8.33-percent-chord-high full-span spoiler. $C_L = 1.02$; $C_D = 0.21$.

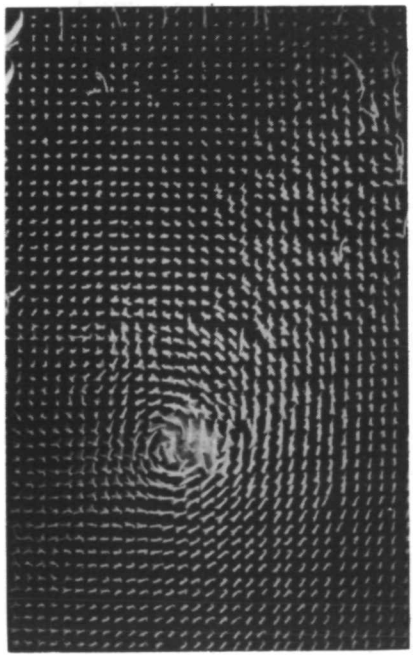

(c) 4.16-percent-chord-high full-span spoiler. $C_L = 1.02$; $C_D = 0.12$.

Figure 9.- Photographs showing effect of full-span and semispan spoilers on tip vortex at 5 chord lengths downstream for near-constant lift coefficient of about 1.0. Spoiler position III; $R = 1.9 \times 10^6$.

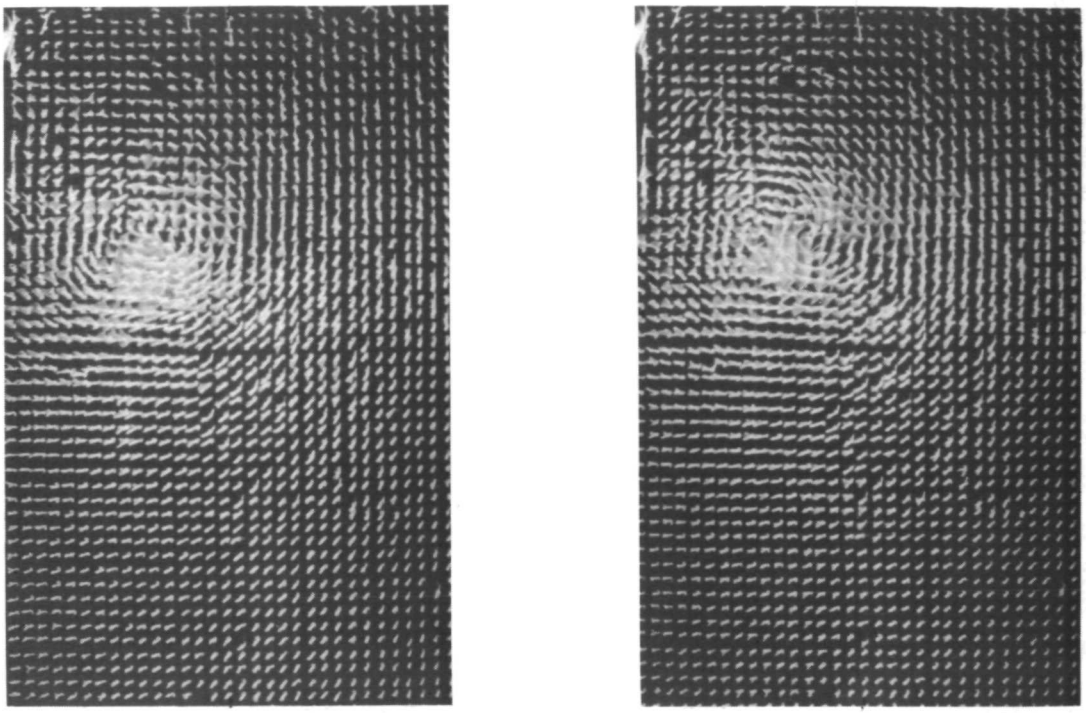

(d) 8.33-percent-chord-high spoiler on semispan outboard. $C_L = 1.02$; $C_D = 0.16$.

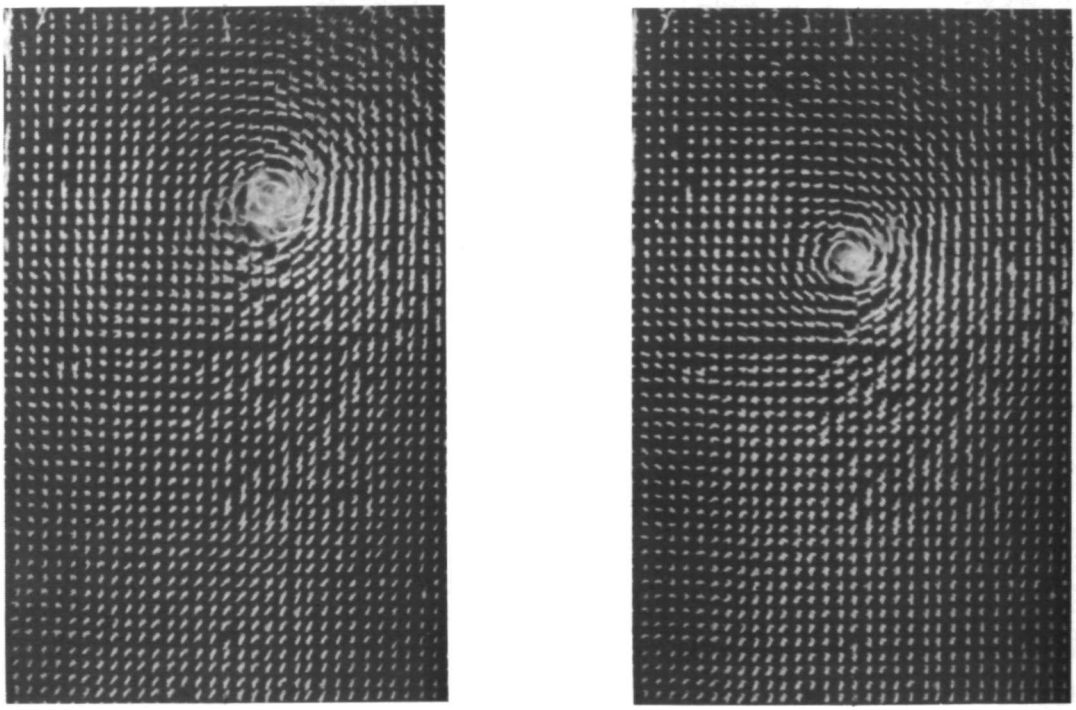

(e) 8.33-percent-chord-high spoiler on semispan inboard. $C_L = 0.99$; $C_D = 0.14$.

Figure 9.- Concluded.

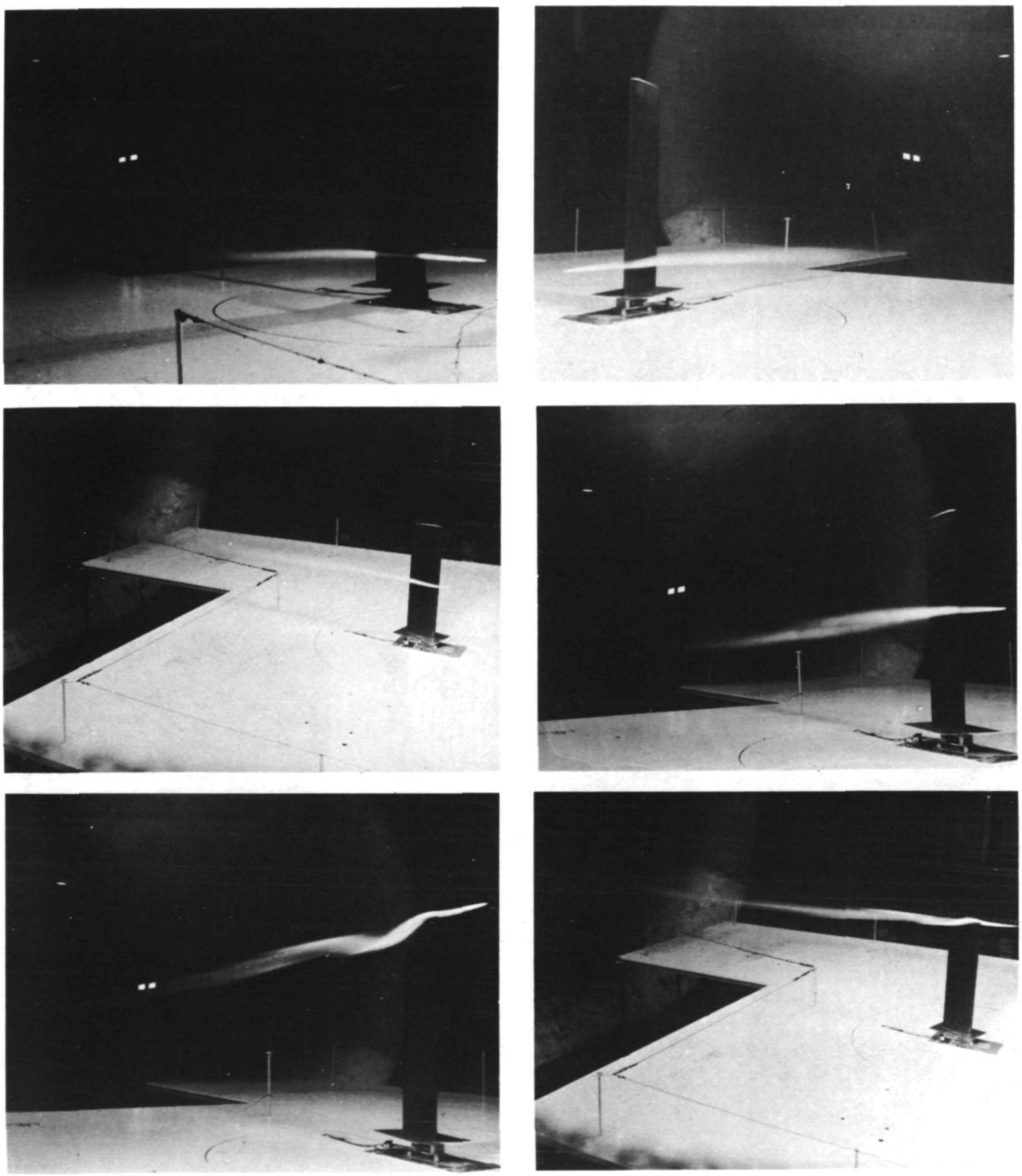

L-72-138

Figure 10.- Photographs of smoke flow with smoke filament at various spanwise stations.

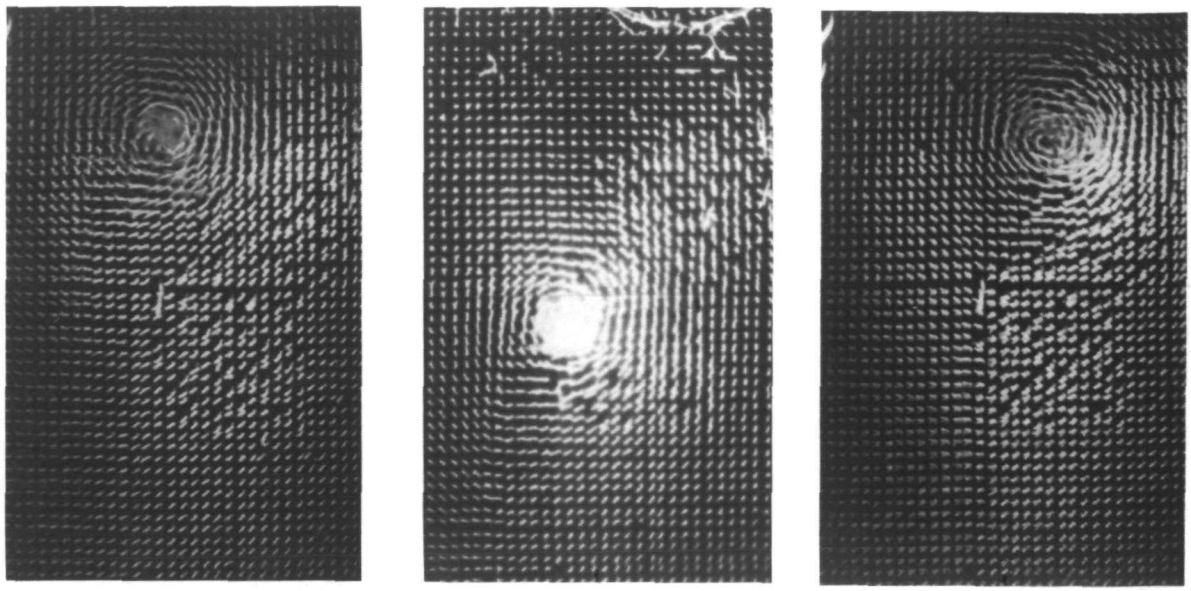

Spoiler position III Clean wing Spoiler position II

(a) Tuft grid at 1 chord length downstream.

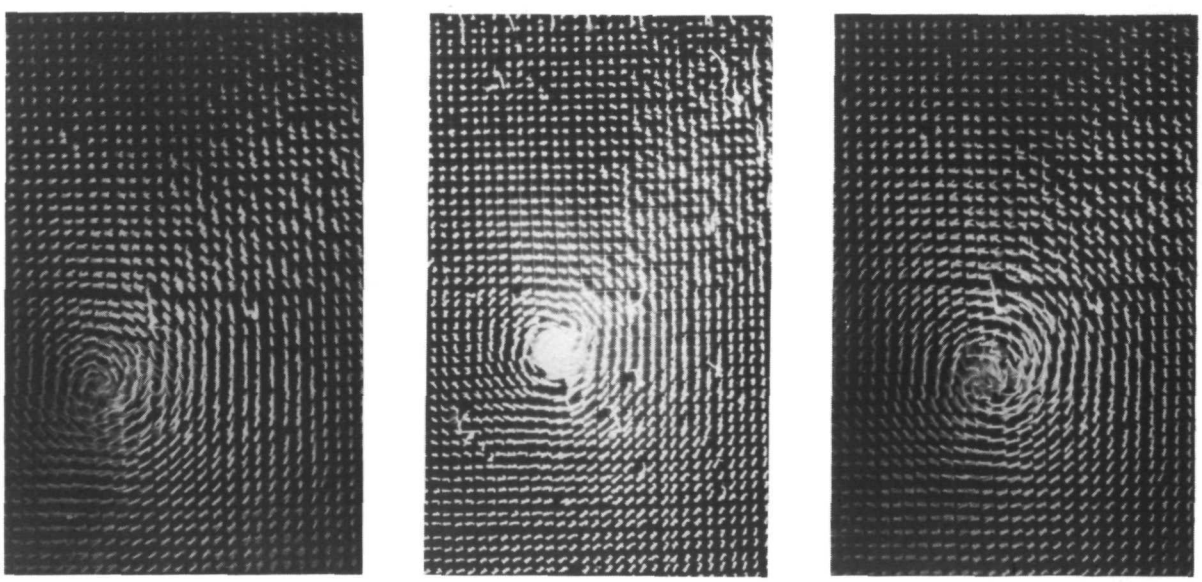

Spoiler position III Clean wing Spoiler position II

(b) Tuft grid at 5 chord lengths downstream.

Figure 11.- Photographs showing effect on tip vortex of 8.33-percent-chord-high 15.2-cm- (6-in-) long spoiler at wing tip. $\alpha = 16.8^{o}$; $R \approx 1.9 \times 10^{6}$.

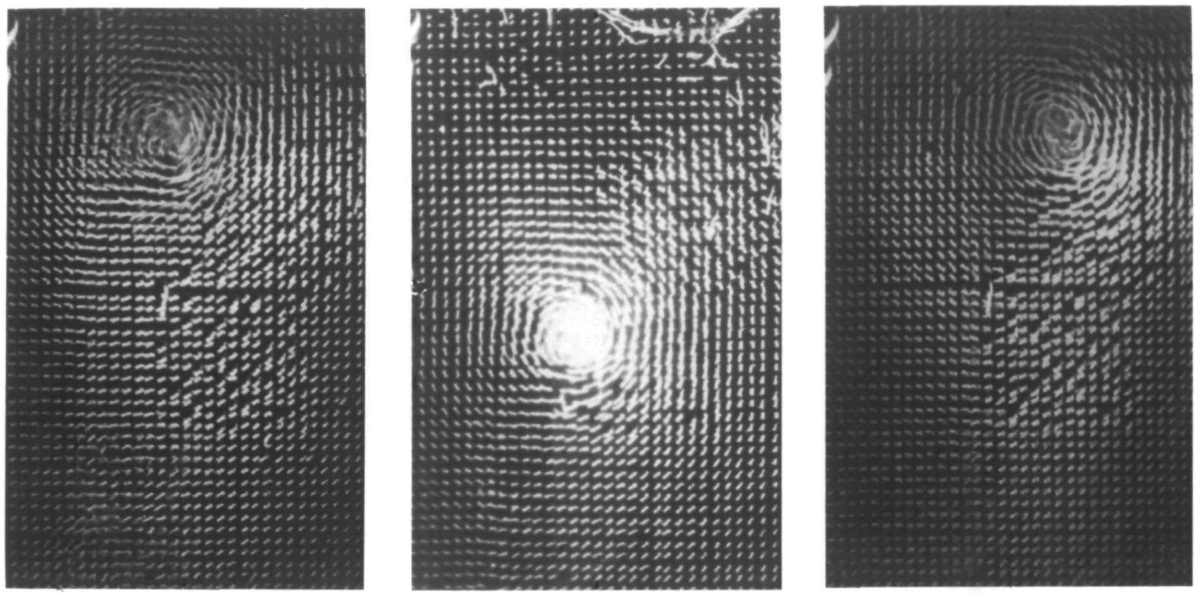

Spoiler position III Clean wing Spoiler position II

(a) Tuft grid at 1 chord length downstream.

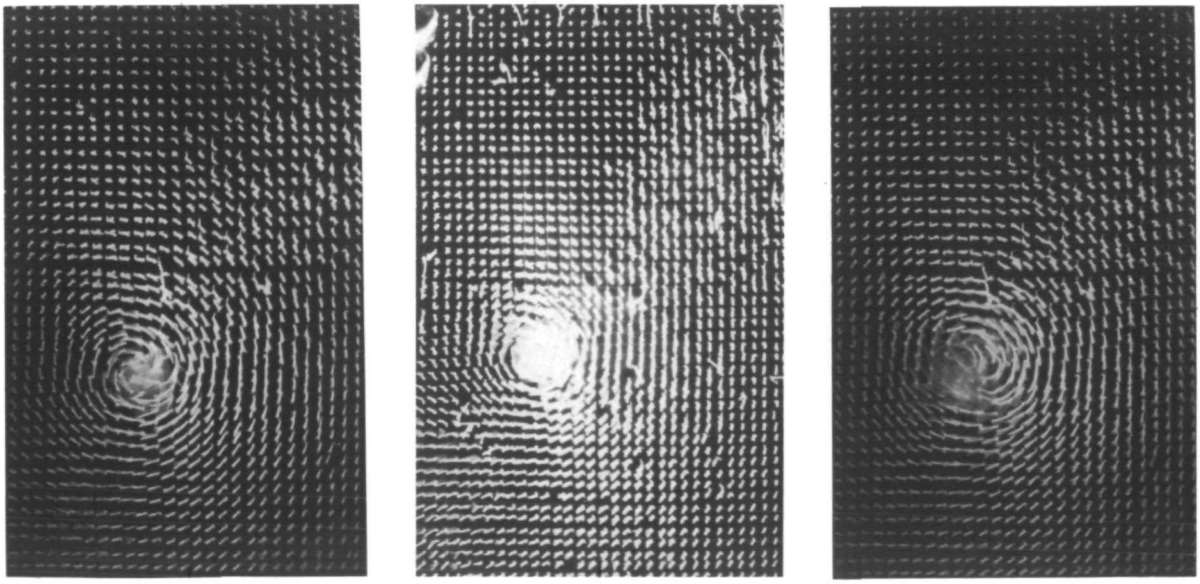

Spoiler position III Clean wing Spoiler position II

(b) Tuft grid at 5 chord lengths downstream.

Figure 12.- Photographs showing effect on tip vortex of 8.33-percent-chord-high 15.2-cm (6-in-) long spoiler at wing tip. $\alpha = 18.8^{\circ}$; $R \approx 1.9 \times 10^{6}$.

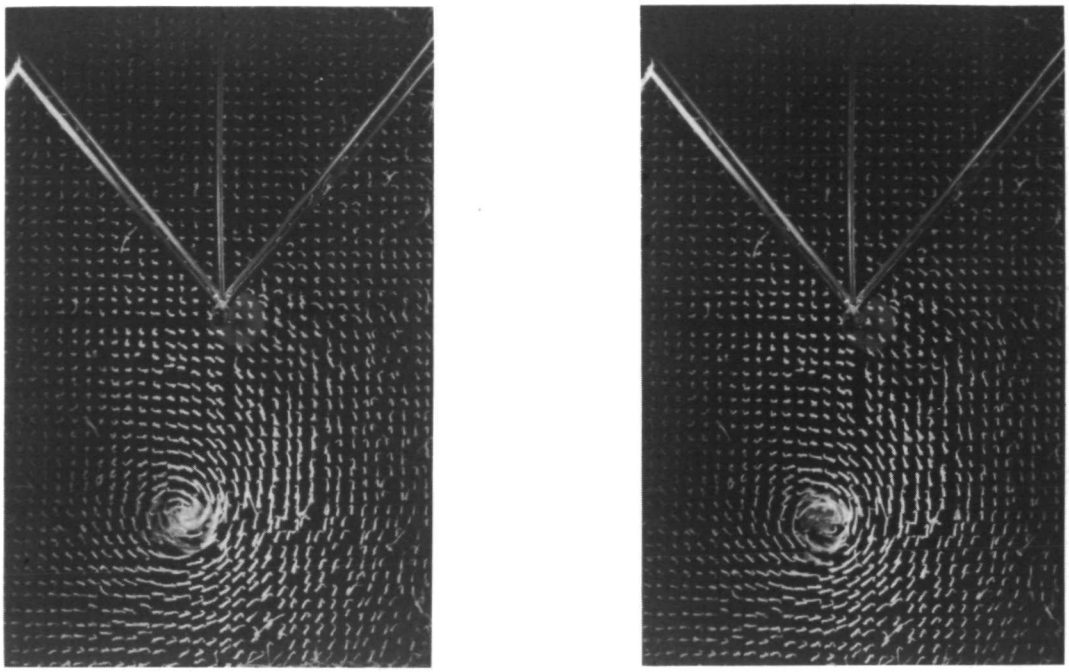

(a) Cone not in (above) vortex core.

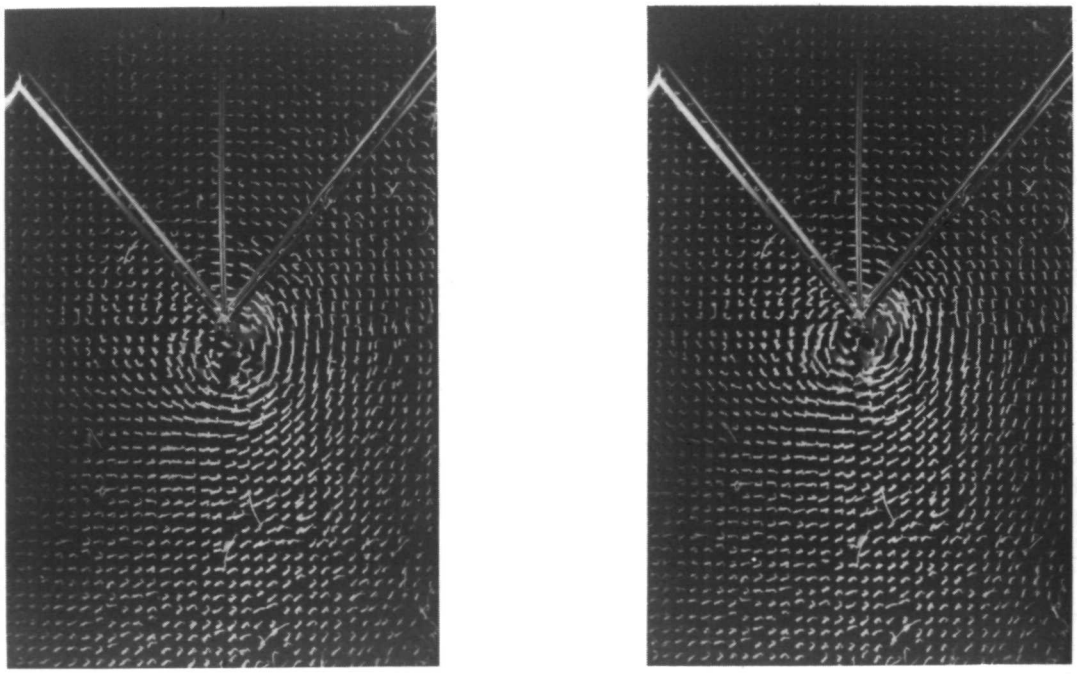

(b) Cone in the vortex core.

Figure 13.- Photographs of tip vortex when cone is placed above or in vortex core. Tuft grid at 5 chord lengths downstream; $\alpha = 16.8^{o}$; $R = 1.9 \times 10^{6}$.

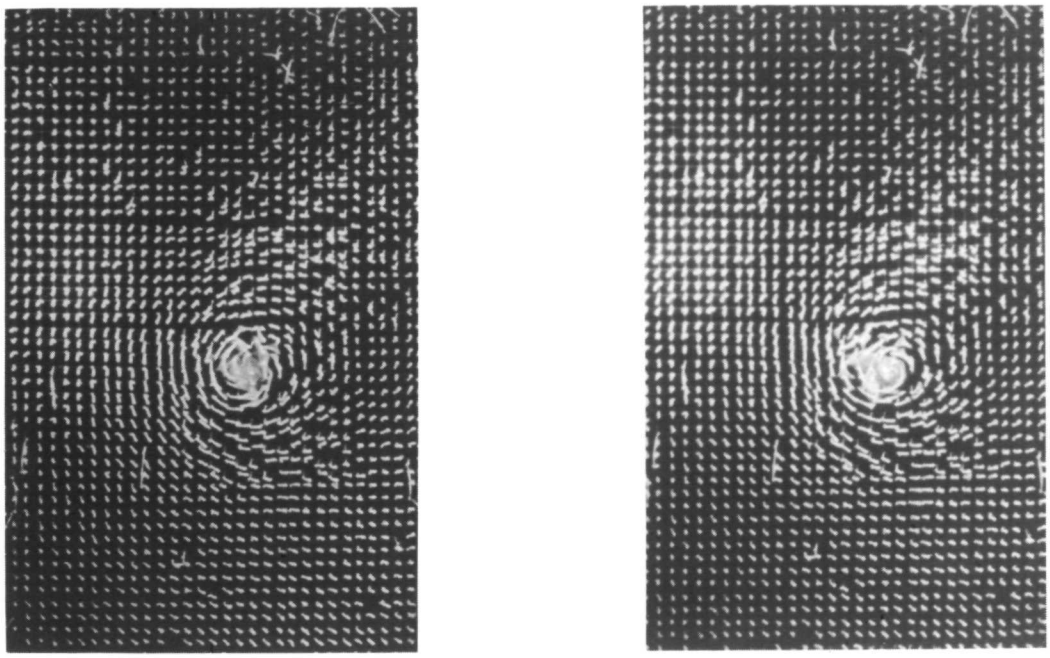

(a) Clean wing. Tuft grid at 5 chord lengths downstream;
$\alpha \approx 13^{o}$; $R \approx 1.2 \times 10^{6}$.

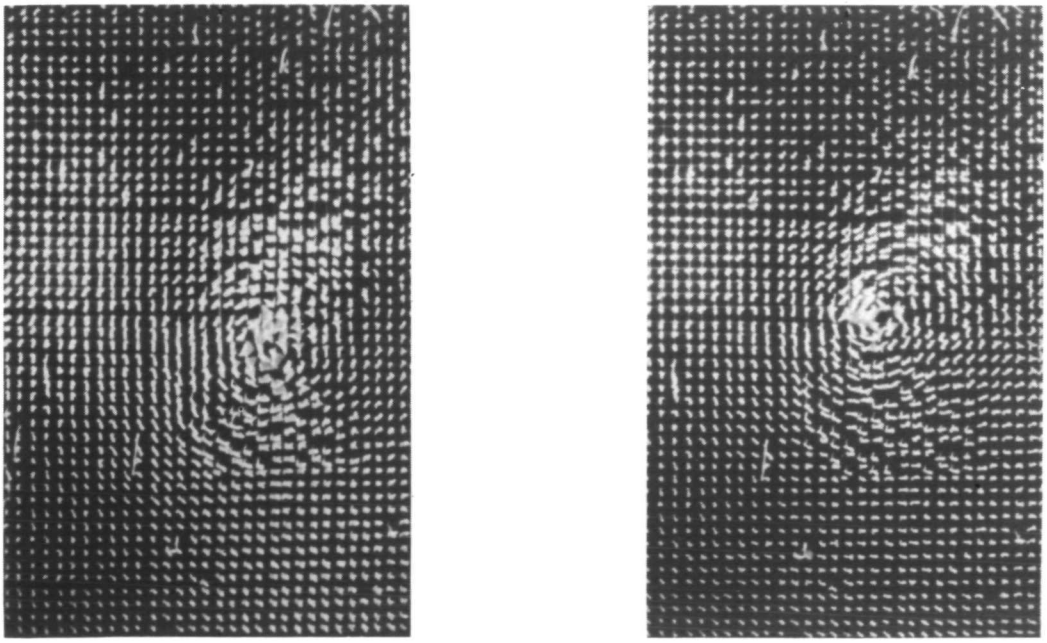

(b) Clean wing with vane attached. Tuft grid at 5 chord lengths downstream;
$\alpha \approx 13^{o}$; $R \approx 1.2 \times 10^{6}$.

Figure 14.- Photographs and tangential-velocity plot showing effect of small vane located about 0.5 chord lengths downstream of wing tip.

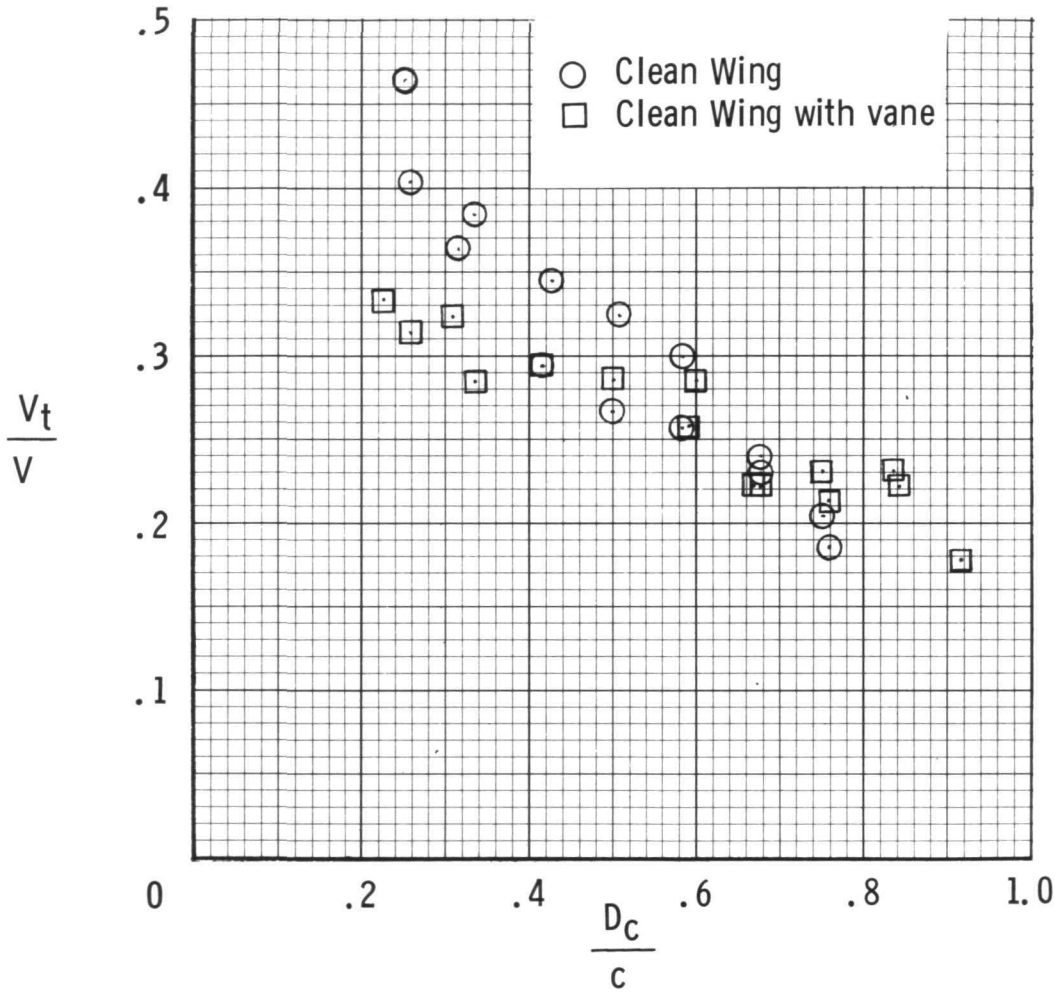

(c) Ratio of tangential velocity to free-stream velocity as a function of ratio of core diameter to wing chord for clean wing with and without vane.

Figure 14.- Continued.

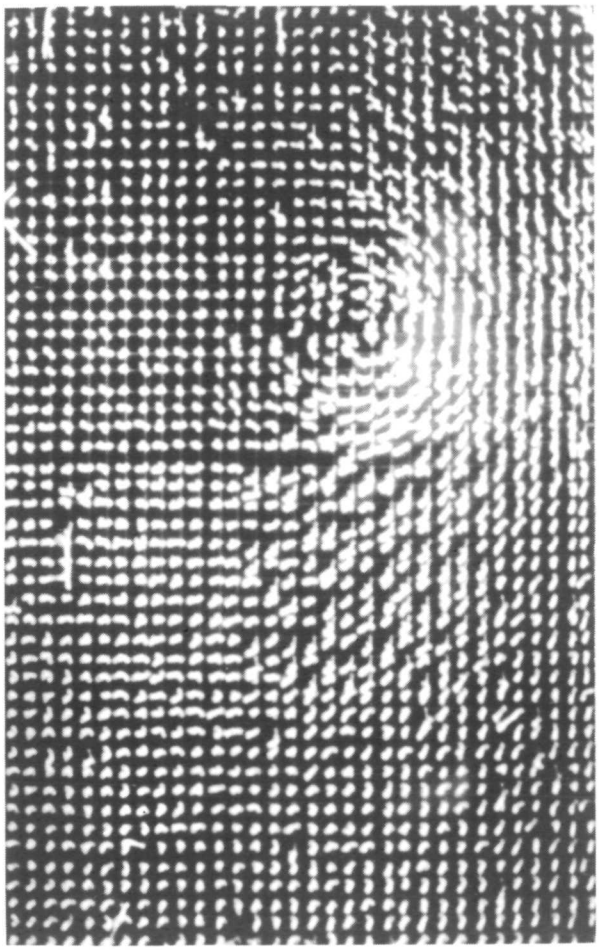

(d) Clean wing with vane attached. Tuft grid at 9 chord lengths downstream; $R \approx 1.9 \times 10^6$; $\alpha \approx 12.8^{\circ}$.

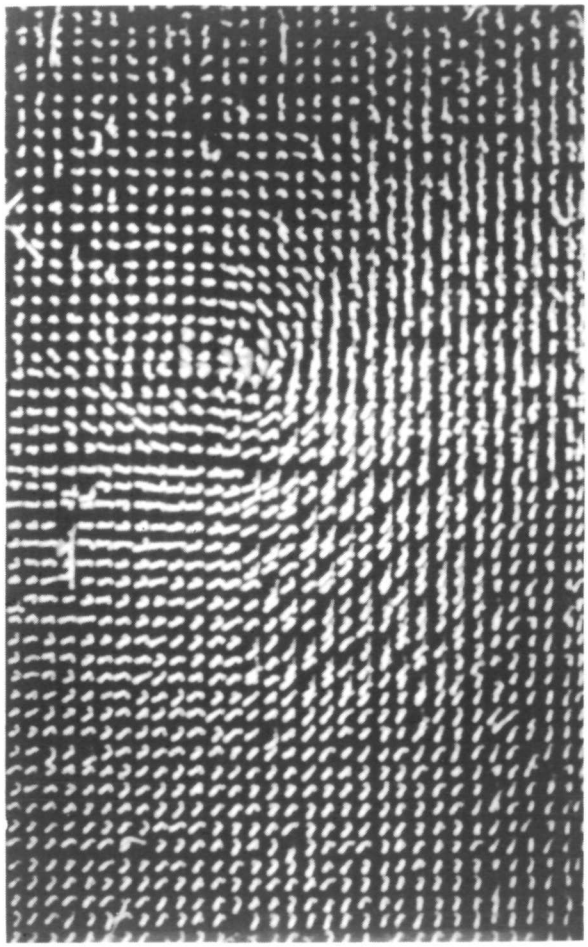

(e) Clean wing with vane attached. Tuft grid at 14 chord lengths downstream; $R = 1.9 \times 10^6$; $\alpha \approx 12.8^{\circ}$.

Figure 14.- Concluded.

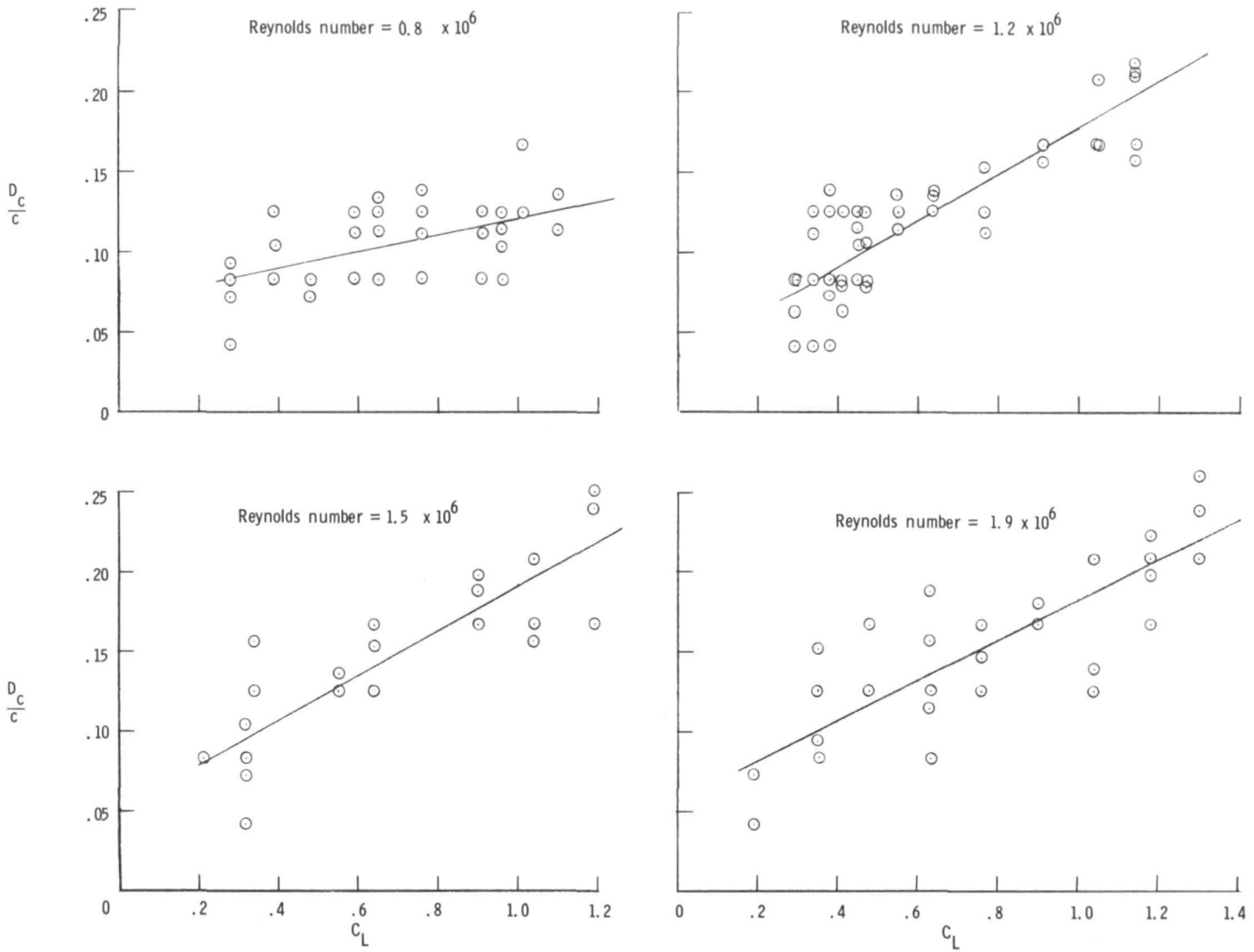

Figure 15.- Variation of core-diameter ratio as a function of C_L for test Reynolds numbers at 5 chord lengths downstream.

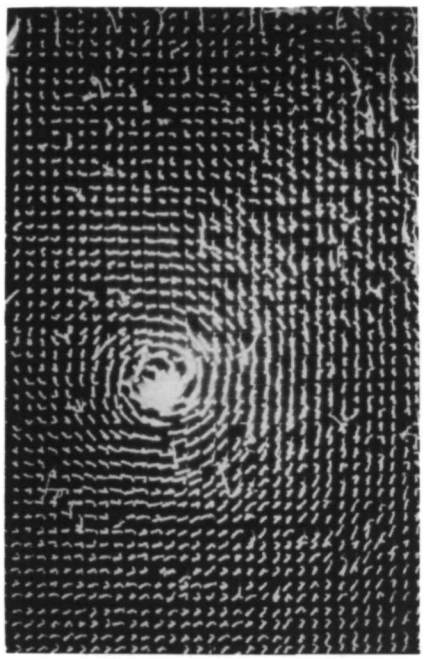

(a) q = 189.6 N/m^2 (3.96 lb/ft^2).

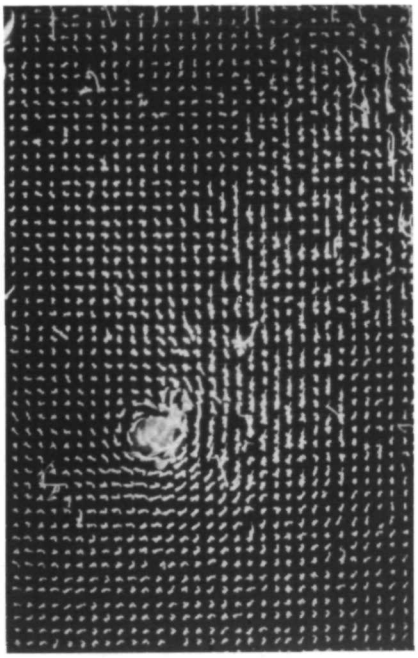

(b) q = 387.8 N/m^2 (8.10 lb/ft^2).

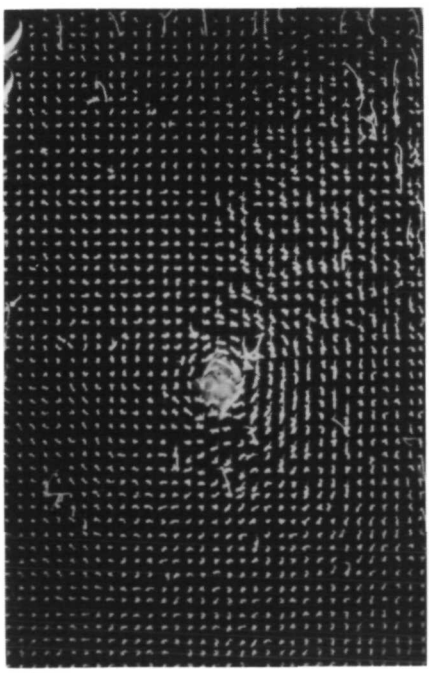

(c) q = 600.9 N/m^2 (12.55 lb/ft^2).

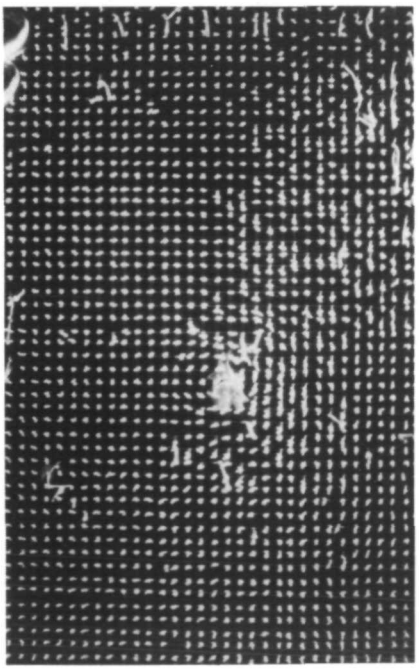

(d) q = 962.9 N/m^2 (20.11 lb/ft^2).

Figure 16.- Photographs of tuft grid showing wing tip vortex for clean wing operating at near-constant lift force of 289 N (65 lb). 5 chord lengths downstream; varying dynamic pressure.

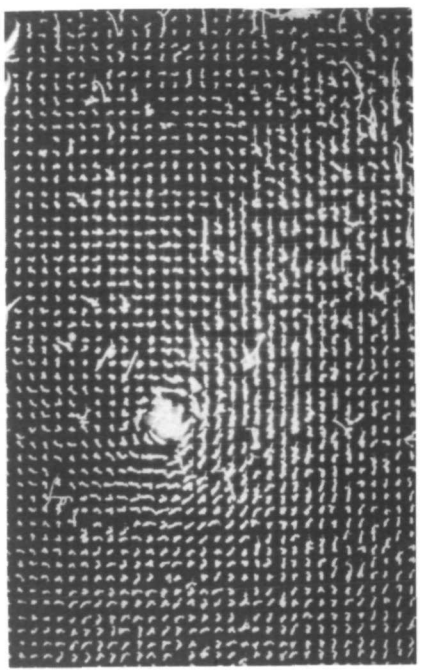

(a) q = 189.6 N/m^2 (3.96 lb/ft^2).

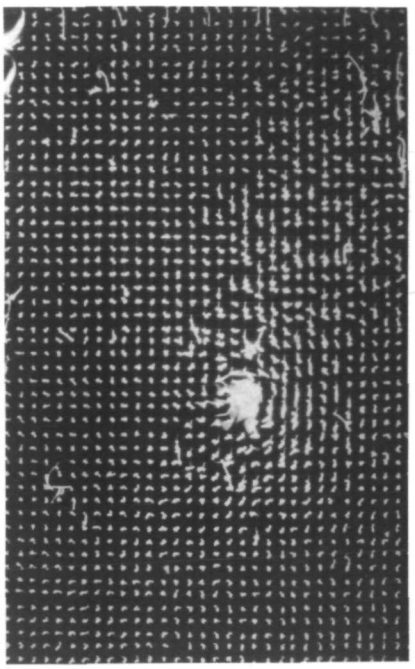

(b) q = 387.8 N/m^2 (8.10 lb/ft^2).

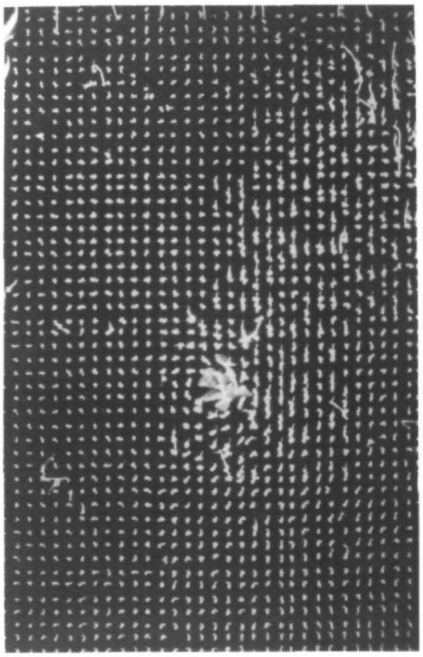

(c) q = 600.9 N/m^2 (12.55 lb/ft^2).

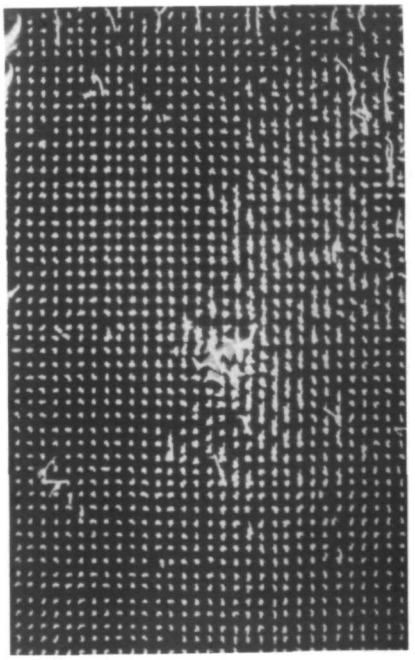

(d) q = 962.9 N/m^2 (20.11 lb/ft^2).

Figure 17.- Photographs of tuft grid showing wing tip vortex for clean wing operating at near-constant lift force of 178 N (40 lb). 5 chord lengths downstream; varying dynamic pressure.

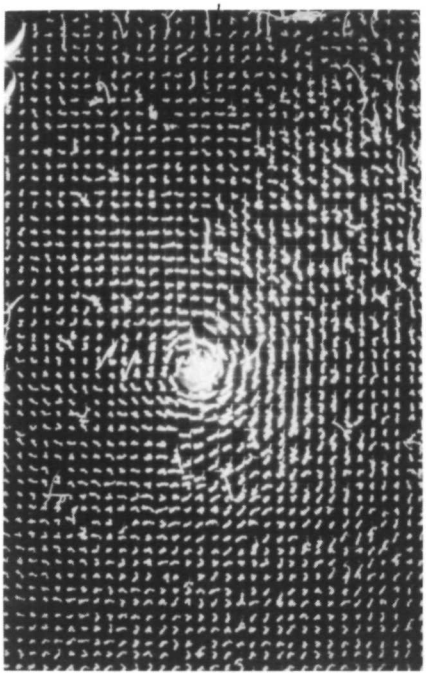

(a) q = 189.6 N/m^2 (3.96 lb/ft^2).

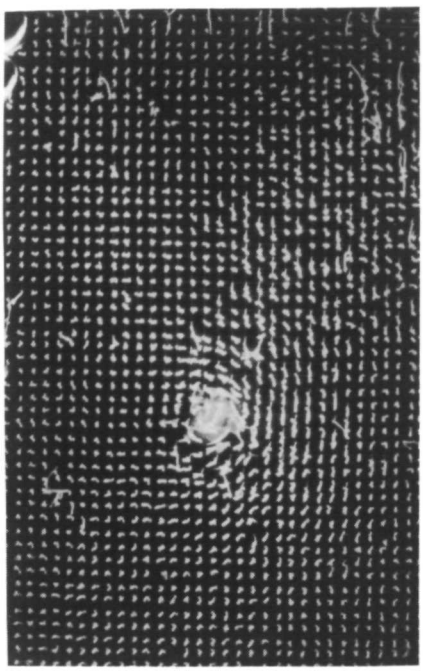

(b) q = 387.8 N/m^2 (8.10 lb/ft^2).

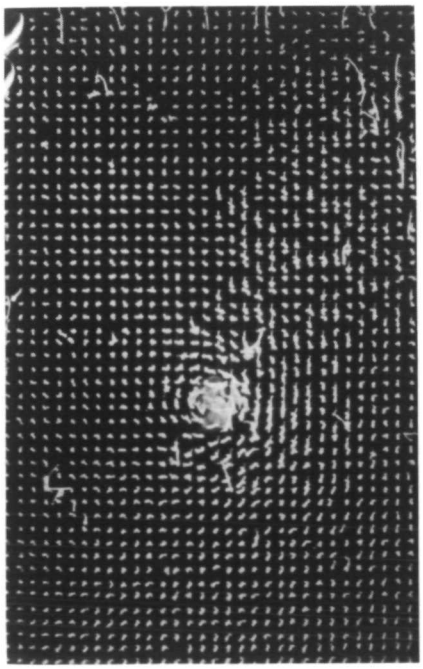

(c) q = 600.9 N/m^2 (12.55 lb/ft^2).

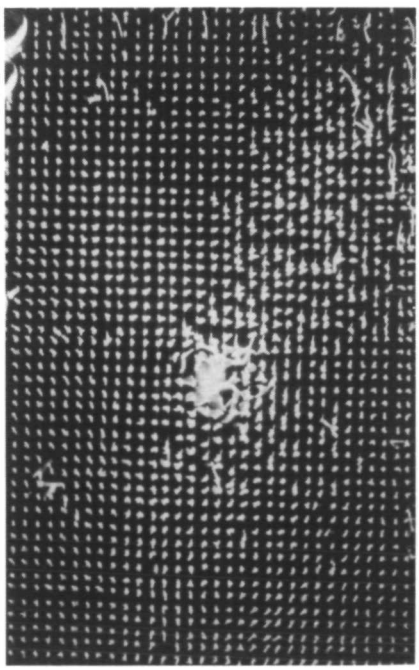

(d) q = 962.9 N/m^2 (20.11 lb/ft^2).

Figure 18.- Photographs of tuft grid showing wing tip vortex for clean wing operating at near-constant circulation of 2.79 m^2/sec (30 ft^2/sec). 5 chord lengths downstream; varying dynamic pressure.

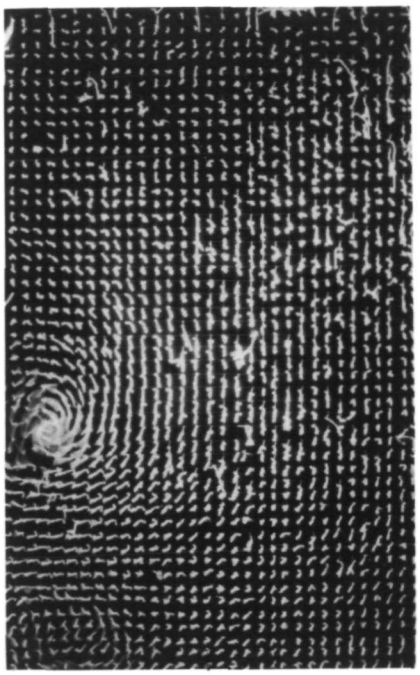

(a) q = 189.6 N/m^2 (3.96 lb/ft^2).

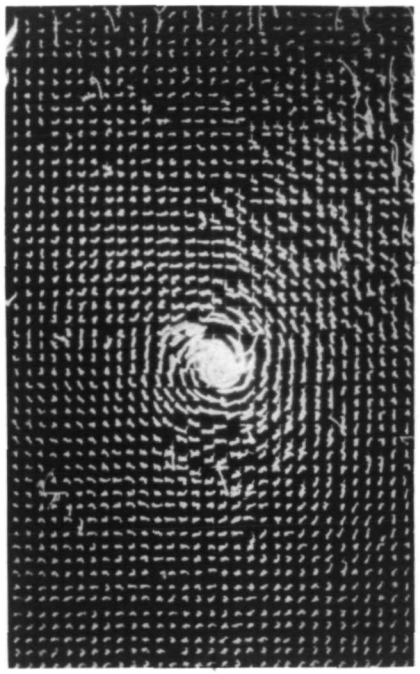

(b) q = 387.8 N/m^2 (8.10 lb/ft^2).

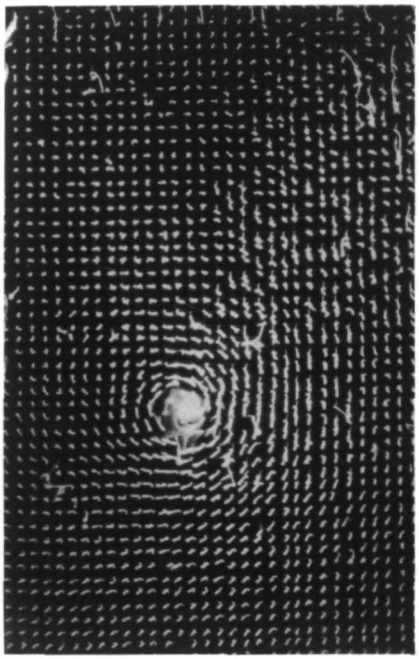

(c) q = 600.9 N/m^2 (12.55 lb/ft^2).

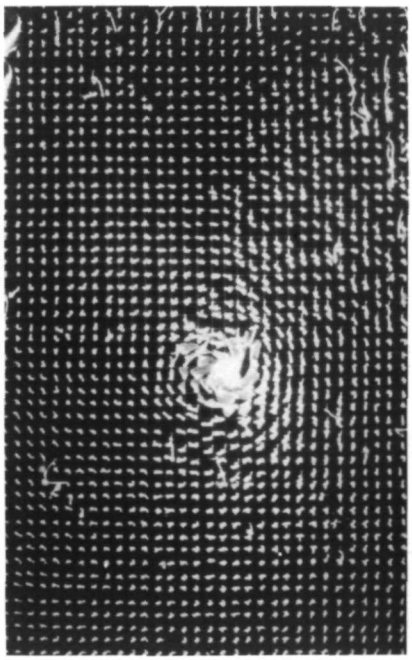

(d) q = 962.9 N/m^2 (20.11 lb/ft^2).

Figure 19.- Photographs of tuft grid showing wing tip vortex for clean wing operating at near-constant circulation of 4.83 m^2/sec (52 ft^2/sec). 5 chord lengths downstream; varying dynamic pressure.

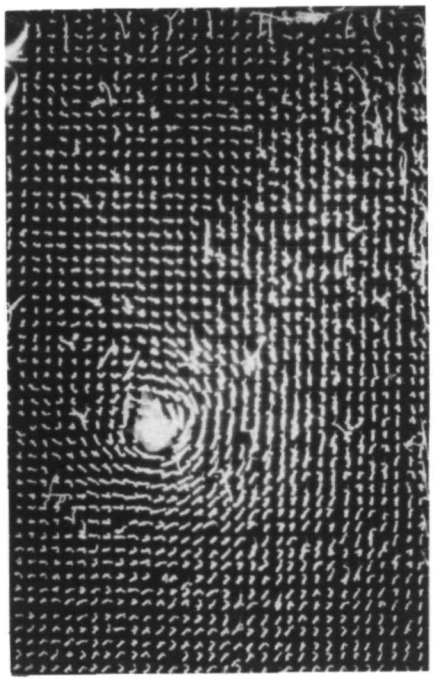

(a) $q = 189.6\ N/m^2$ $(3.96\ lb/ft^2)$.

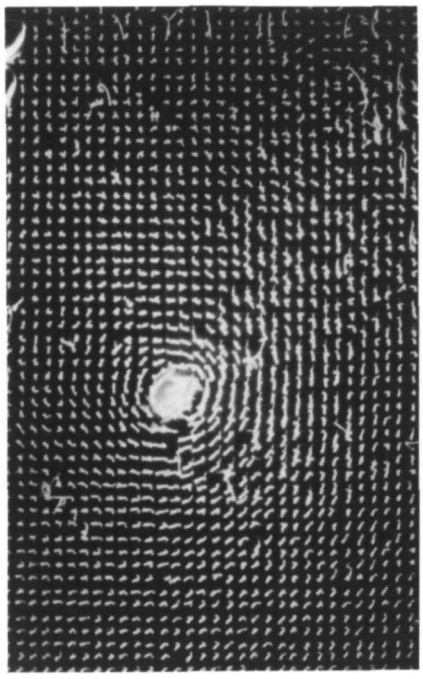

(b) $q = 387.8\ N/m^2$ $(8.10\ lb/ft^2)$.

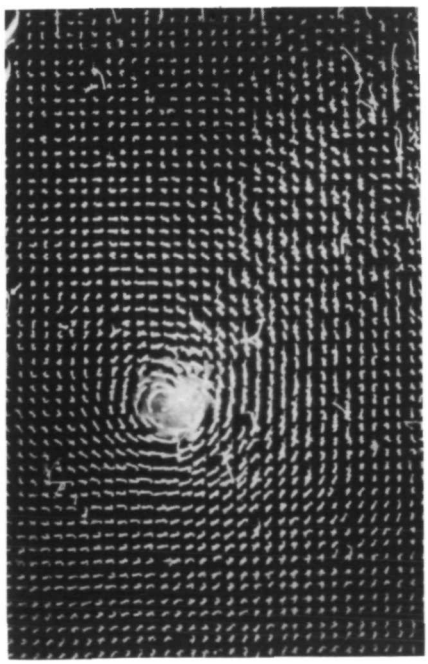

(c) $q = 600.9\ N/m^2$ $(12.55\ lb/ft^2)$.

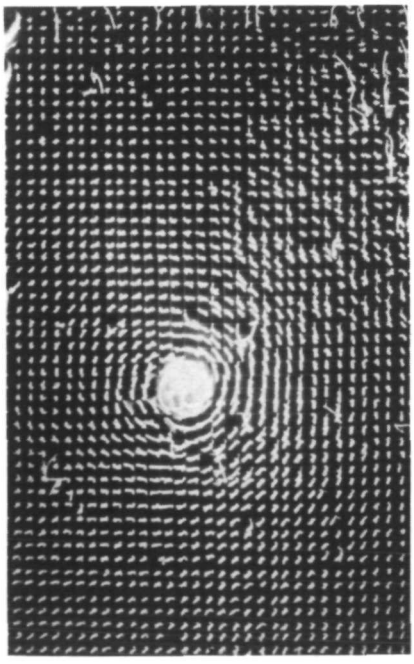

(d) $q = 962.9\ N/m^2$ $(20.11\ lb/ft^2)$.

Figure 20.- Photographs of tuft grid showing wing tip vortex for clean wing operating at near-constant lift coefficient of 0.91. 5 chord lengths downstream; varying dynamic pressure.

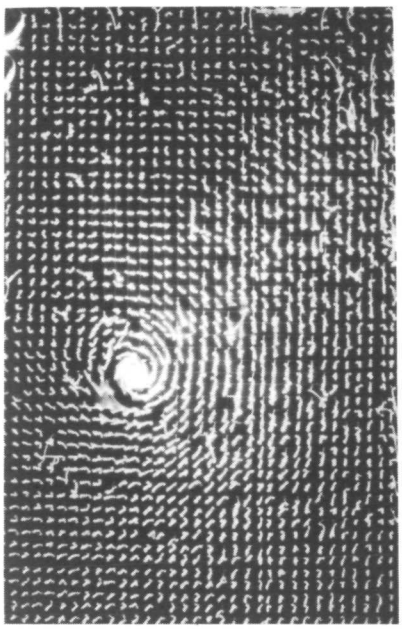

(a) $C_L = 0.95$;
$q = 189.6\ N/m^2$
$(3.96\ lb/ft^2)$.

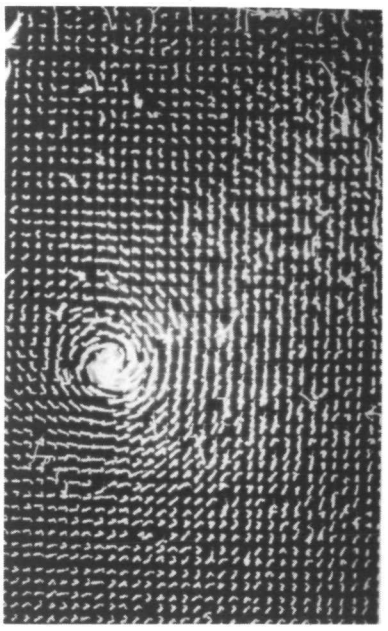

(b) $C_L = 1.10$;
$q = 189.6\ N/m^2$
$(3.96\ lb/ft^2)$.

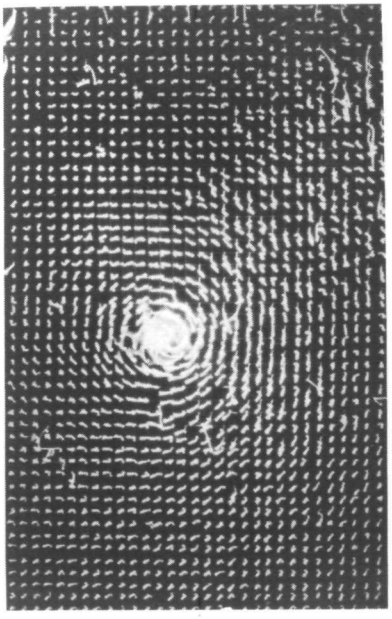

(c) $C_L = 1.04$;
$q = 387.8\ N/m^2$
$(8.10\ lb/ft^2)$.

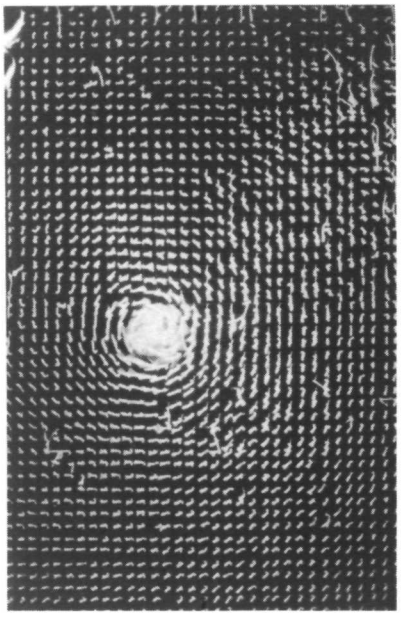

(d) $C_L = 1.04$;
$q = 600.9\ N/m^2$
$(12.55\ lb/ft^2)$.

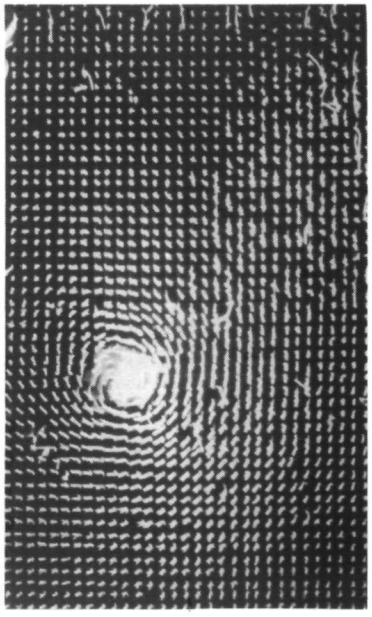

(e) $C_L = 1.04$;
$q = 962.9\ N/m^2$
$(20.11\ lb/ft^2)$.

Figure 21.- Photographs of tuft grid showing wing tip vortex for clean wing operating at near-constant lift coefficient of 1.04. 5 chord lengths downstream; varying dynamic pressure.

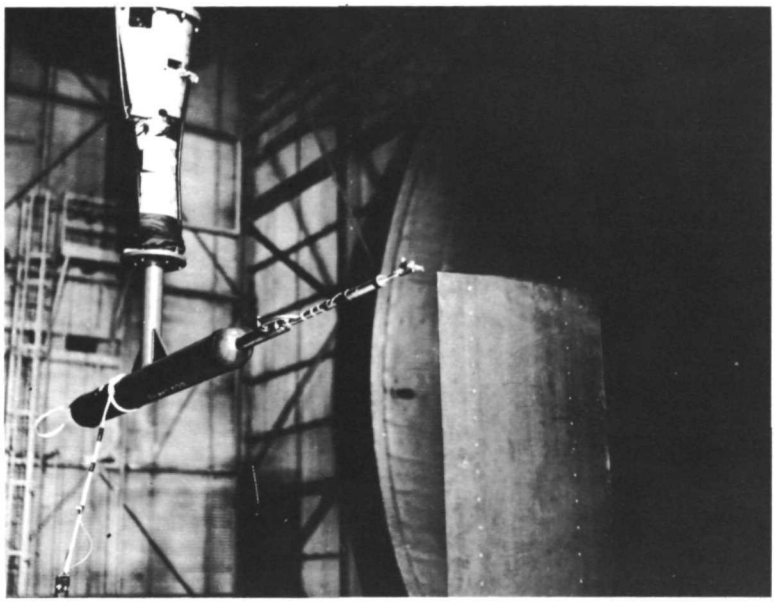

(a) Vorticity meter mounted behind wing.

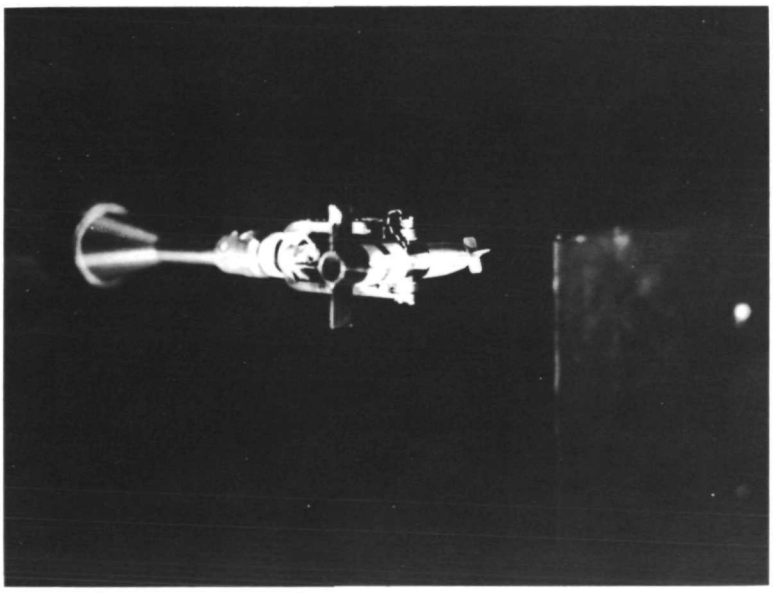

L-72-139

(b) Vorticity meter.

Figure 22.- Photographs of vorticity meter.

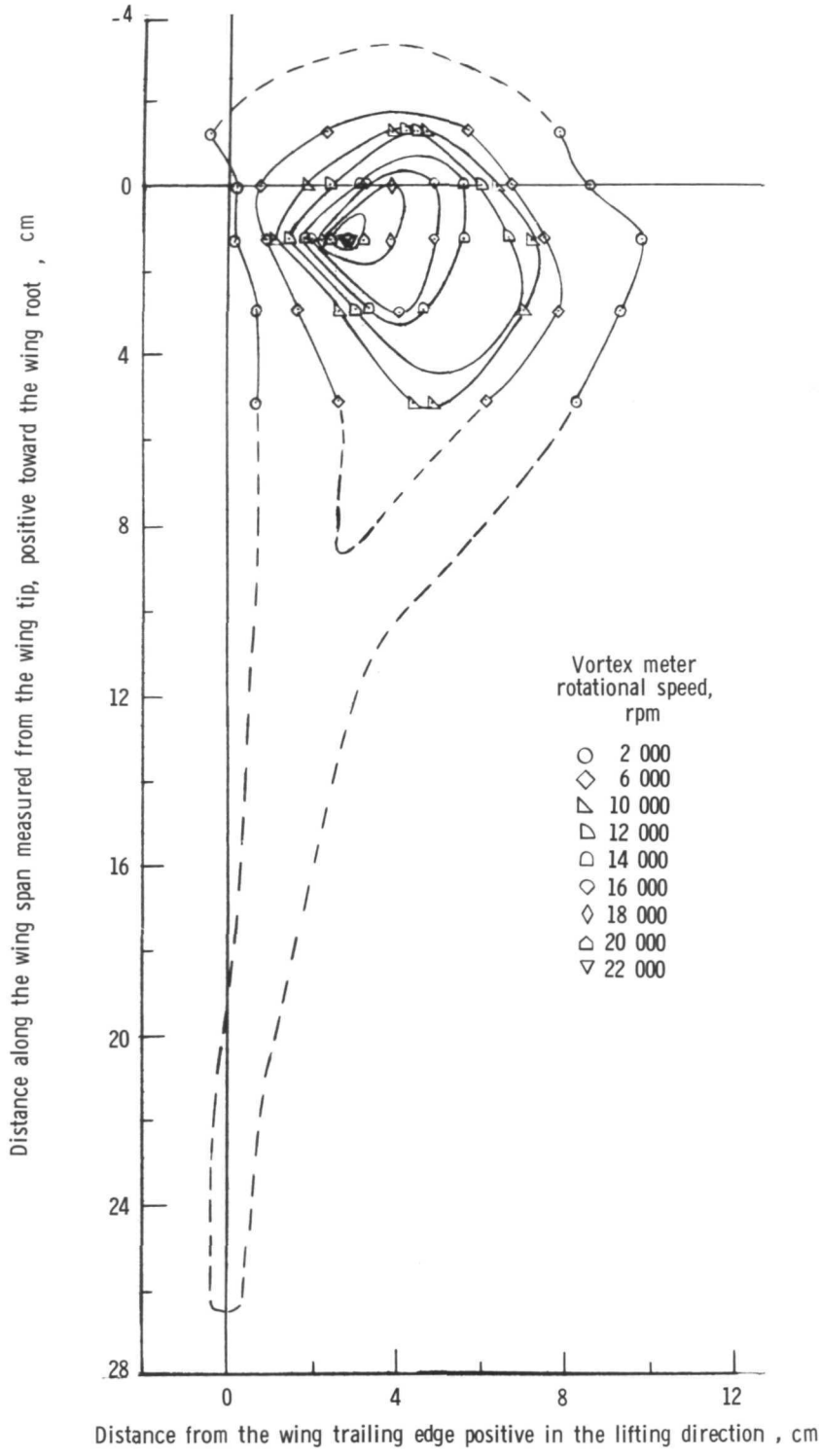

Figure 23.- Typical map of rotational speed as measured by vorticity meter at 1 chord length from trailing edge of wing and at $\alpha = 12.8^{o}$ and $q = 962.9\ N/m^2$ (20.11 lb/ft^2).

NASA-Langley, 1972 —— 1 L-8104

Page Intentionally Left Blank

Page Intentionally Left Blank

Page Intentionally Left Blank

A motion-picture film supplement L-1113 is available on loan. Requests will be filled in the order received. You will be notified of the approximate date scheduled.

The film (16 mm, 17.5 min, color, silent) documents, with a smoke-flow visualization technique, the wing tip-vortex flow pattern generated by a semispan-wing model having an NACA 0012 airfoil section with a 0.61-meter (2-foot) chord and set at 12° angle of attack. Illustrations are presented for the wing tip clean, with spoilers on the lower surface, with an end plate on the wing tip, with a solid object (cone) in the vortex core, and with a vane located 0.5 chord behind the wing in the vortex core.

Requests for the film should be addressed to:

NASA Langley Research Center
Att: Photographic Branch, Mail Stop 171
Hampton, Va. 23365

CUT

Date _____

Please send, on loan, copy of film supplement L-1113 to TM X-2516.

_____
Name of organization

_____
Street number

_____
City and State Zip code

Attention: Mr. _____

Title _____

CUT

Place
Stamp
Here

NASA Langley Research Center
Att: Photographic Branch, Mail Stop 171
Hampton, Va. 23365

"The aeronautical and space activities of the United States shall be conducted so as to contribute . . . to the expansion of human knowledge of phenomena in the atmosphere and space. The Administration shall provide for the widest practicable and appropriate dissemination of information concerning its activities and the results thereof."

—NATIONAL AERONAUTICS AND SPACE ACT OF 1958

NASA SCIENTIFIC AND TECHNICAL PUBLICATIONS

TECHNICAL REPORTS: Scientific and technical information considered important, complete, and a lasting contribution to existing knowledge.

TECHNICAL NOTES: Information less broad in scope but nevertheless of importance as a contribution to existing knowledge.

TECHNICAL MEMORANDUMS: Information receiving limited distribution because of preliminary data, security classification, or other reasons.

CONTRACTOR REPORTS: Scientific and technical information generated under a NASA contract or grant and considered an important contribution to existing knowledge.

TECHNICAL TRANSLATIONS: Information published in a foreign language considered to merit NASA distribution in English.

SPECIAL PUBLICATIONS: Information derived from or of value to NASA activities. Publications include conference proceedings, monographs, data compilations, handbooks, sourcebooks, and special bibliographies.

TECHNOLOGY UTILIZATION PUBLICATIONS: Information on technology used by NASA that may be of particular interest in commercial and other non-aerospace applications. Publications include Tech Briefs, Technology Utilization Reports and Technology Surveys.

Details on the availability of these publications may be obtained from:

SCIENTIFIC AND TECHNICAL INFORMATION OFFICE

NATIONAL AERONAUTICS AND SPACE ADMINISTRATION

Washington, D.C. 20546